Environ Monit Assess (2023) 195:175
https://doi.org/10.1007/s10661-022-10719-z

Seasonal changes of trace elements, nutrients, dissolved organic matter, and coastal acidification over the largest oyster reef in the Western Mississippi Sound, USA

M. S. Sankar · Padmanava Dash · YueHan Lu · Xinping Hu · Andrew E. Mercer · Sudeera Wickramarathna · Wondimagegn T. Beshah · Scott L. Sanders · Zikri Arslan · Jamie Dyer · Robert J. Moorhead

Received: 13 May 2022 / Accepted: 5 November 2022

Abstract Seasonal changes of trace elements, nutrients, dissolved organic matter (DOM), and carbonate system parameters were evaluated over the largest deteriorating oyster reef in the Western Mississippi Sound using data collected during spring, summer, and winter of 2018, and summer of 2019. Higher concentrations of Pb (224%), Cu (211%), Zn (2400%), and Ca (240%) were observed during winter of 2018 compared to summer 2019. Phosphate and ammonia concentrations were higher (> 800%) during both summers of 2018 and 2019 than winter of 2018. Among the three distinct DOM components identified, two terrestrial humic-like components were more abundant during both spring (12% and 36%) and summer (11% and 33%) of 2018 than winter of 2018, implying a relatively lesser supply of humic-like components from terrestrial sources during winter. On the other hand, the protein-like component was more abundant during summer of 2019 compared to rest of the study period, suggesting a higher rate

Highlights
- Water quality over the oyster reef is seasonally and hydrologically controlled.
- The trace elements were higher during spring and winter of 2018 than summer 2019.
- Three dissolved organic matter components were identified over the oyster reef.
- Significant seasonal change in carbonate system parameters was observed.
- The water over the oyster reef was above the saturation state of $CaCO_3$ (> 1).

Supplementary Information The online version contains supplementary material available at https://doi.org/10.1007/s10661-022-10719-z.

M. S. Sankar · R. J. Moorhead
Geosystems Research Institute, Mississippi State University, Mississippi State, MS 39762, USA

M. S. Sankar · X. Hu
Harte Research Institute for Gulf of Mexico Studies, Texas A&M University-Corpus Christi, Corpus Christi, TX 78412, USA

P. Dash (✉) · A. E. Mercer · S. Wickramarathna · W. T. Beshah · S. L. Sanders · J. Dyer
Department of Geosciences, Mississippi State University, Mississippi State, MS 39762, USA
e-mail: pd175@msstate.edu

Y. Lu
Department of Geological Sciences, University of Alabama, Tuscaloosa, AL 35487, USA

X. Hu
Department of Physical and Environmental Sciences, Texas A&M University-Corpus Christi, Corpus Christi, TX 78412, USA

Z. Arslan
MS 973, Federal Center, U.S. Geological Survey, Denver, CO 80225, USA

Published online: 05 December 2022

of autochthonous production during summer 2019. In addition, to their significant depth-wise variation, ocean acidification parameters including pH, pCO_2, CO_3^{2-}, and carbonate saturation states were all higher during both summers of 2018 and 2019. The measured variables such as trace elements, organic carbon, suspended particulates, and acidification parameters exhibited conservative mixing behavior against salinity. These observations have strong implications for the health of the oyster reefs, which provides ecologically important habitats and supports the economy of the Gulf Coast.

Keywords Watershed biogeochemistry · Oyster health · Water quality · Dissolved organic matter · Coastal acidification · Northern Gulf of Mexico

Introduction

The economy of the southern coastal states of the USA depends on shellfish production to a great extent (Weber & Mitchell, 2013). Coastal waters of the Mississippi Sound are rich habitats for oysters as well as fish, and commercially harvestable oyster reefs covering an area of 7400 acres (30 km^2) exist along the western portion of the Mississippi Sound (Mississippi Department of Environmental Quality, 2015). However, pollution in the coastal waters is causing deterioration of the oyster reefs and possible extinction in the near future (Beck et al., 2011). Studies indicate that declining water quality in the region has caused the mortality of more than 86% of oysters in the Western Mississippi Sound (Kennicutt, 2017; La Peyre et al., 2014; Mississippi Department of Environmental Quality, 2015). As per the Mississippi Gulf Coast restoration plan, water quality degradation of the region has been linked to multiple factors, such as freshwater incursions, nutrient input from terrestrial sources, hurricanes, and oil spills, while the exact cause and mechanism remain unclear.

The health of oyster reefs is tightly coupled with a range of water quality indicators as well as with various environmental processes that mediate water quality (Beck et al., 2011). Studies indicate that high turbidity and lower dissolved oxygen in the surrounding waters can cause oyster mortality (Lunt & Smee, 2014; Sarinsky et al., 2005; Soletchnik et al., 2007). Additionally, freshwater influx and corresponding changes in salinity and temperature can also cause oyster mortality (Powell et al., 2003; Rajagopal et al., 2005; Soletchnik et al., 2007). Excessive phytoplankton biomass, as measured by chlorophyll-*a* concentration, can adversely affect oyster health through bottom water hypoxia caused by heterotrophic respiration. For example, higher chlorophyll-*a* concentrations during summer months led to a higher mortality rate in juvenile oysters; while in the autumn–winter period, the elevated chlorophyll-*a* concentrations led to the death of 2-year-old oysters along the coasts of France (Soletchnik et al., 2007). Similarly, seasonal precipitation in the watershed and associated water discharge into the coastal oceans can cause significant salinity changes and can lead to oyster mortality (La Peyre et al., 2013; Soletchnik et al., 2007). Additionally, pathogens and fungal diseases could also lead to a higher rate of oyster mortality (Andrews, 1984; Andrews & Hewatt, 1967; Winstead & Couch, 1988). Oysters can also act as hyper-accumulators of trace elements if the surrounding water body is contaminated, which could adversely affect the health of both oysters and their consumers (García-Rico et al., 2003; Wang et al., 2018). Dissolved organic matter (DOM) can form complexes with trace elements and aggravate the toxicity effects on the early life stages of the oysters (Brooks et al., 2007). Changes in the balance of the production and remineralization of DOM can influence the concentration of CO_2, pH, and O_2 in the water, which can have significant impacts on oysters (Cai et al., 2011). The absorption of light by chromophoric DOM (CDOM) in the ultraviolet and blue portions of the spectrum makes it an important control on the transfer of solar radiation through the water column, which is critical to the structure and function of aquatic ecosystems including oyster reefs (Häder et al., 2007). Similarly, excessive input of nutrients into coastal waterbodies from adjacent watersheds can lead to algal blooms and/or seasonal hypoxia and ultimately to oyster mortality (Hagy et al., 2004; Keppel et al., 2016). Last but not the least, coastal acidification can adversely affect oyster health by causing high mortality rates in oyster larvae and also inhibiting shell formation (Waldbusser et al., 2015, 2016).

The water quality of a region has been traditionally assessed using a suite of indicators that directly relate

to the stress of an ecosystem. Measurement of the indicators such as salinity, water temperature, depth and transparency of the water, trace element concentration, nutrient concentration, quantity and quality of dissolved organic matter (DOM), and acidification parameters can reveal information about the water quality and its effect on the surrounding aquatic ecosystem. Additionally, linking the temporal changes of the indicators mentioned above with watershed hydrology, weather conditions, biological activity, and land use and land cover of the surrounding watershed would reveal biogeochemical mechanisms responsible for the water quality variation in the aquatic environment (Lu et al., 2014a; Sankar et al., 2019a). Several studies have been conducted to understand watershed biogeochemical mechanisms influencing water quality by linking water chemistry with the surrounding watershed environment (Beck et al., 2011; Lu et al., 2014b; Sankar et al., 2019a; Sarinsky et al., 2005). Hydrogeological studies conducted along the coastal regions of the Northern Gulf of Mexico along Louisiana, Mississippi, and Alabama indicate that the combination of seasonal weather patterns and inland anthropogenic activities including agricultural and industrial effluents regulate the movement of trace elements, nutrients, and DOM, thus affecting the coastal water quality (Alexander et al., 2008; Bianchi et al., 2007; Chen & Gardner, 2004; Faust et al., 2018; Sankar et al., 2019a; Singh et al., 2018).

A few studies have been conducted to evaluate the water quality of the Mississippi sound and its influence on oyster health (Runner & Floyd, 2002; Soniat, 2014; Turner, 2006), but a systematic study of the seasonal change in water quality and its relationship with the surrounding coastal watersheds is lacking. This study was carried out to evaluate the seasonal variation of water quality over the largest oyster reef of the Western Mississippi Sound by combining field, laboratory, and spatial data. Water quality assessment was performed using a comprehensive suite of indicators, including trace elements, calcium (Ca), nutrients, DOM quantity and composition, and coastal acidification parameters. The main objectives were to (a) evaluate the seasonal variation of water quality and identify those variables that exert significant control over the oyster health, and (b) determine the biogeochemical mechanisms responsible for the changes in water quality proximal to the oyster reefs.

Materials and methods

Site description, fieldwork, sample processing, and hydrological data acquisition

The Mississippi Sound extends in an east–west direction along the Florida-Alabama-Mississippi-Louisiana coastal tract in the northern Gulf of Mexico (Fig. 1). It is a shallow (~3–4-m depth) elongated basin with minimal tidal influence (<0.6 m) covering an area of 4792 km^2 separated from the Gulf of Mexico by a series of small sand bars and islands with an average freshwater inflow of 1235 m^3s^{-1} (Cambazoglu et al., 2017; USEPA, 1999). This is an important nursery area for commercial and recreational fishing, seagrass beds, and various estuarine-dependent species including loggerhead sea turtles and shellfish (Beccasio, 1982). Coastal watersheds including North Lake Pontchartrain, Pearl-Bogue Chitto, Mississippi Coastal, Pascagoula Basin, Mobile River Basin, and Perdido Basin border the northern side of the Mississippi Sound. Rivers such as Pearl River from the Pearl-Bogue Chitto watershed, Wolf River, Jourdan River, Red Creek, and Cypress Creek from the Mississippi Coastal watershed, Pascagoula River predominantly from the Pascagoula Basin, Mobile River from the Mobile River Basin, and Perdido River from the Perdido Basin discharge into the Mississippi Sound. Additionally, water from Lake Pontchartrain of North Lake Pontchartrain watershed, and sometimes Mississippi River water diverted through the Bonnet Carré Spillway to Lake Pontchartrain empties into the Western Mississippi Sound. The area where water samples were collected covers 15.25 km^2 of the Mississippi Sound and overlies the largest oyster reef stretching from the mouth of the Bay St. Louis to Pass Christian in Western Mississippi Sound (Fig. 1).

Water samples along with salinity, water temperature, Secchi depth, water depth, and sampling location information were collected from 70 different locations distributed over the study area spanning four field campaigns during spring (March 13–15, May 7–10), summer (June 19–20, July 16–20), and winter (December 17–18) seasons of 2018 and the summer of 2019 (June 15–19, July 29–August 2). A total of 31 surface samples were collected during spring 2018, while a total of 14 samples were collected during summer 2018 and 7 samples were collected during winter 2018. Additionally, 18 more

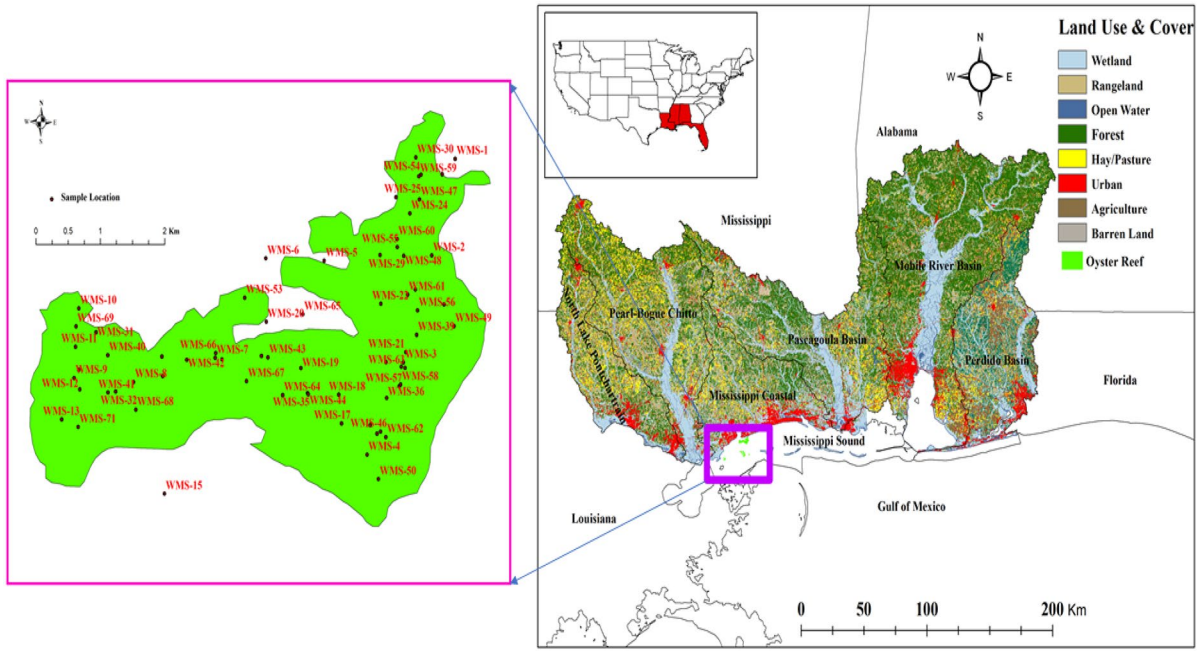

Fig. 1 Land use and land cover map of six watersheds bordering the study area (right). The oyster reef with sampling points indicated (left)

samples were collected during summer 2019. Surface water samples for the subsequent analysis of trace elements, Ca, nutrients, DOM, and suspended particulate matter (SPM) were collected using a 12-ft extendable swing sampler rod with the attachment of acid-washed 1-L high-density polyethylene (HDPE) bottles (Dash et al., 2015; Sankar et al., 2019a). Additionally, water samples for the carbonate chemistry parameters were collected in 250-mL borosilicate glass bottles with 100 µL saturated mercury chloride (Fisher Scientific®, $HgCl_2$) solution from the top, middle, and bottom depths from all locations using a Niskin water sampler (Cai et al., 2017). Although the sampling depth varied at each location, the surface sample was designated as the top, while the middle sample at each location was collected by taking sample at the halfway of the total depth followed by a sample from the bottom of the water column. Except the first sampling trip in March 2018, when only surface samples were collected, otherwise water samples were collected from top, middle, and bottom depths. Along with sample collection, the depth profiles of salinity and water temperature were measured using a HANNA® probe from each sample location. After collection, samples were stored in a cooler filled with ice and transported to the lab for processing and storage.

In the lab, a portion of the collected surface water samples was filtered through 0.2-µm Whatman® nuclepore track-etch membrane filters into separate acid-washed, and oven-dried 20-mL VWR® HDPE narrow mouth bottles for the analysis of trace elements, Ca, nutrients, and DOC. The water samples for trace elements and Ca were acidified using Fisherbrand® ultrapure nitric acid (0.2% by volume) and were stored at room temperature, while the samples for nutrients, DOC, and TDN were stored in a freezer at − 80 °C. Additionally, 50 mL of the filtered surface samples was stored in 100-mL Fisherbrand® acid-washed and pre-combusted amber glass bottles for CDOM UV–Vis absorption and fluorescence measurements and refrigerated at 4 °C. Another portion of the surface water samples in replicates was used for SPM analysis. Water samples were brought to ambient room temperature prior to laboratory analysis.

Hydrological data including river discharge and precipitation in the watersheds were collected from US Geological Survey (USGS) National Water Information System Web Interface and multi-sensor precipitation estimates (MSPE) derived from hourly

Weather Surveillance Doppler Radar-1988 (WSR-88D) for the study period from January 2018 to December 2019. Available daily discharge data for the rivers draining through the six watersheds bordering the Western Mississippi Sound were collected from respective USGS measuring stations, including Pearl River (USGS 02,489,500), Wolf River (USGS 02,481,510), Red Creek (USGS 02,479,300), Cypress Creek (USGS 02,479,155), Pascagoula River (USGS 02,479,000), Mobile River (USGS 02,470,629), and the Perdido River (USGS 02,376,500). Discharge through the Bonnet Carré Spillway opening for the years 2018 and 2019 were collected from the US Army Corps of Engineers Bonnet Carré Spillway overview website. The total daily precipitation in each of the six watersheds was calculated from hourly precipitation data with 4×4 km^2 spatial resolution in Python and ArcGIS following the procedure explained in Dyer and Mercer (2013).

The land use and land cover (LULC) classes of six watersheds bordering the Western Mississippi Sound were obtained from the geospatial data gateway of the United States Department of Agriculture (USDA). The individual watersheds were delineated by overlaying the digital elevation model (DEM), the hydrological unit code-8 (HUC-8) watershed boundary dataset along with the stream dataset of the state of Florida, Alabama, Mississippi, and Louisiana in ArcGIS® 10.3.1 software platform. The LULC information of the individual watersheds was extracted by overlaying selected polygons of the HUC-8 watershed boundaries over the LULC layers of the individual states (Fig. 1).

Analysis of water samples for trace elements, nutrients, and suspended particulate matter

The concentrations of trace elements in the water samples, including arsenic (As), manganese (Mn), copper (Cu), lead (Pb), zinc (Zn), and uranium (U), and a major element calcium (Ca) were determined by inductively coupled plasma mass spectrometry (ICP-MS) using a Varian 820MS ICP-MS instrument located at Jackson State University as per the analytical procedures described elsewhere (Paul et al., 2021). National Institute of Standards and Technology (NIST) freshwater certified reference material (SRM 1640a, Trace Elements in Natural Water) was analyzed in triplicate for quality control purposes. Values from SRM 1640a ($n = 3$) were within 95% confidence level of the certified values and/or reference values. The concentration of dissolved nutrients including phosphate (PO_4^{3-}), nitrate (NO_3^-), ammonium (NH_4^+), and nitrite (NO_2^-) was analyzed using a continuous flow auto-analyzer (Skalar Analytical Inc., Buford, GA) at Dauphin Island Sea Lab. The DOC concentrations in each of the water samples were measured on a SHIMADZU® total organic carbon-total nitrogen analyzer (TOCv-TNM1) equipped with an ASI-V autosampler following the method described in Shang et al. (2018). The SPM content was analyzed following the Glass-fiber filter (GFF) method, B-3401–85 (Guy & Norman, 1970). Specifically, well-mixed 200 mL of surface water samples in duplicates were filtered using pre-combusted (500 °C), pre-washed, and oven-dried 47-mm Whatman® GF-F filters. Along with the samples, blank controls were also processed by filtering 18.2 MΩ deionized water (Barnstead). After filtration, filters were oven-dried at 105 °C. After drying, the filters were weighed and stored inside clean aluminum foils and again weighed before ashing at 500 °C in a Thermo Scientific® Lindberg/Blue M BF51748C muffle furnace. The total quantity (mg/L) of SPM, suspended inorganic matter (SPIM, calculated as SPM-SPOM), and suspended organic matter (SPOM, calculated using the mass difference before and after ashing) were calculated.

Analysis of carbonate system parameters

Carbonate system parameters including pH, dissolved inorganic carbon (DIC), and total alkalinity (TA) were analyzed at the School of Marine Science and Policy, University of Delaware, USA, following the analytical procedures in Cai et al. (2017). The partial pressure of carbon dioxide (pCO_2), bicarbonate (HCO_3^-), and carbonate (CO_3^{2-}) and the concentration of dissolved carbon dioxide (CO_2(aq)), aragonite saturation state (Ω_{Ar}), and calcite saturation state (Ω_{Ca}) were calculated using MS-Excel program CO2SYS-V2.1 using pH and DIC as input parameters. Constant selections were as the following: K_1, K_2 from Mehrbach et al. (1973) and refit by Dickson and Millero (1987); K_2SO_4 from Dickson (1990); and total boron from Uppström (1974). The pH was reported on the NBS scale.

CDOM characterization by measurement of optical indices and PARAFAC modeling

Optical characteristics of the 70 water samples collected were determined by employing absorption and fluorescence measurements. Absorption spectra of the water samples were measured using a Lambda 850 double-beam spectrophotometer (PerkinElmer®, Waltham, MA, USA). Wavelengths between 200 and 750 nm were captured at every 2-nm intervals in a clean 4-mL quartz cuvette with 1-cm path length. From the blank-corrected absorbance (A) values, the Napierian absorption coefficient (a, m^{-1}) for each sample at every wavelength (λ) was calculated (Sankar et al., 2019b). Absorption indices such as UV absorption coefficient at 254 nm ($a254$), UV absorption coefficient at 440 nm ($a440$), the ratio of UV absorption coefficient at 250 to 365 or $a250$:$a365$ (E2:E3), and spectral slope ratio (SR) for each of the samples were calculated from the absorption coefficients (Hansen et al., 2016; Sankar et al., 2020; Singh et al., 2018). SR was calculated as the ratio of the spectral slopes of $a275$–295 nm to that of $a350$–400 nm. Furthermore, by dividing the $a254$ values by DOC concentration, the specific UV absorbance ($SUVA_{254,}$ Lmg^{-1} m^{-1}) was calculated. The $SUVA_{254}$ values indicate aromaticity, while values of both E2:E3 and SR are inversely proportional to the molecular weight of DOM (Dalrymple et al., 2010; Hansen et al., 2016; Sankar et al., 2019a; Singh et al., 2018; Spencer et al., 2013). The values of $a440$ are directly proportional to CDOM concentration (Sankar et al., 2020; Singh et al., 2017a).

The excitation-emission-matrices (EEM) fluorescence spectra were collected using a Fluoromax-4 spectrofluorometer (Horiba Jobin Yvon Inc., Edison, NJ, USA). The EEMs were collected in signal to noise ratio (S_1^c/R_1^c) mode after applying excitation peak, emission peak, cuvette contamination, Raman Peak checks, and instrument-specific corrections and calibrations. Emissions were recorded between 300 and 550 nm at 2-nm intervals and 0.25-s integration time with EEM excitations between 240 and 450 nm at 10-nm increments with a 5-nm slit width. The EEMs were blank-corrected, Raman-normalized, and adjusted for inner filter effects prior to the computation of fluorescence indices and parallel factor (PARAFAC) modeling (Sankar et al., 2019b). The calculation of fluorescence index (FI), humification index (HIX), and biological index (BIX) followed the steps in Hansen et al. (2016). FI values indicate the source of DOM with values between 1.6 and 2.0 indicating a microbial origin and values between 1.2 and 1.5 indicating a terrestrial origin, i.e., from decayed terrestrial plants and soils (McKnight et al., 2001). HIX indicates the degree of humification of natural organic matter (Sankar et al., 2019a), and larger values suggest strong humification with contraction of fluorescent molecules or low H/C ratios of DOM (Ohno, 2002). BIX measures the freshness of DOM, higher BIX values (>1) indicate freshly released autochthonous production, while lower BIX (0.6–0.7) indicates the dominance of allochthonous produced compounds (Parlanti et al., 2000).

A total of 70 sample EEMs, representing spring 2018 ($n=31$), summer 2018 ($n=14$), winter 2018 ($n=7$), and summer 2019 ($n=18$) were used for PARAFAC modeling, following the procedure described in Stedmon and Bro (2008). Preceding the modeling, all 70 EEMS were normalized to Raman-integrated area at 350-nm excitation and 397-nm emission over 5-nm bandpass. After removing two outliers (two abnormal spring 2018 samples), a three-component PARAFAC model was created and validated by split-half analysis using Tucker congruence coefficients and random initialization method. The results of three-component PARAFAC scores were represented as fluorescence intensity maximum (F_{max}) in Raman units (R.U). The PARAFAC computations were performed using the DOMFluor toolbox in MATLAB®-R2018a computing platform (Stedmon & Bro, 2008).

Statistical data analysis

The statistical analysis was performed in the R-version 3.3.2 (R Core Team, 2016) programming platform. Bootstrap resampling and non-parametric tests were applied because the assumption of normality (data fitting the bell-shaped curve) was not met for this dataset. Bootstrapping is a non-parametric resampling method with replacement to get normally distributed data from which the confidence intervals of the variables can be computed to estimate significant differences and similarities. The mean and standard deviation were calculated, and box plots were created for all the measured variables. Subsequently, bootstrap resampling at confidence intervals of 2.5% (lower quartile), 50% (median), and 97.5% (upper

quartile) was applied to water temperature, salinity, trace elements, Ca, nutrients, SPM, carbonate system parameters, DOC, DOM optical indices, and PARAFAC components to evaluate if they vary significantly with season by taking 1000 means or replicates; subsequently, the replicates were used for creating boxplots. If there are any significant differences ($p < 0.05$), then the bootstrap median value of an event does not lie within the limits of 2.5% and 97.5% limits of the other events. Readers may refer to Table 2 for seasonal averages; Figs. 3, 5, and SI Fig. 1 for seasonal variations, and SI Figs. 2, 3, 4, and 6 for bootstrap results. Spearman rank correlation was applied to F_{max} of the PARAFAC components and the optical indices to assess the correlation of the source and composition of DOM, with the correlation coefficient classified as strong ($r \geq 0.7$), moderate ($0.7 \geq r \geq 0.5$), or weak ($0.5 \geq r \geq 0.3$). A *t*-test was performed to estimate the significance of slope for changes in dissolved constituents with salinity for investigating the extent and behavior of mixing. Principal component analysis (PCA) was performed to assess significant differences and sample grouping due to season and to reveal the underlying biogeochemical processes. All statistical analyses were performed at a 95% confidence level (p-value < 0.05). Finally, Spearman's rank correlation was performed for the winter 2018 subset to further evaluate the explicit association of trace elements (Cu, Mn, As, Pb, Zn, U), Ca, SPM, SPIM, and SPOM in the PCA plot.

Results

Watershed characteristics, seasonal change in precipitation, and discharge

Among the six watersheds bordering the northern side of the study area, the Mobile River Basin watershed was the largest (11,586 km^2), which covers parts of Alabama and Mississippi; while North Lake Ponchartrain watershed covering parts of Louisiana and Mississippi was the smallest (3825 km^2). Areas of all the watersheds are given in SI. Table 1. The largest landcover class in all the watersheds were forests, followed by wetlands (Fig. 1). The combined areal coverage of agriculture and pasture was high in Perdido Basin (12.8% and 5.25%, respectively), Pearl-Bogue Chitto (2.41%; 12.2%), North Lake Ponchartrain (3.57%; 10.8%), and Pascagoula Basin (2.35%; 7.19%) watersheds, while slightly higher areal coverage of urbanized areas was present in both Mississippi Coastal (12.8%) and North Lake Ponchartrain (10.6%) watersheds compared to the rest.

The average discharge of the seven rivers was highest during the winter of 2018 and lowest during the summer of 2018 (Table 1). When comparing the seven rivers of the study area, the Mobile River always had the highest discharge, and the Cypress Creek had the lowest discharge. The average water discharge during winter 2018 through the rivers in the ascending order were Cypress Creek (5.29 ± 9.45 m^3s^{-1}), Perdido River (28.9 ± 15.9 m^3s^{-1}), Wolf River (29.8 ± 29.4 m^3s^{-1}), Red Creek (42.0 ± 30.8 m^3s^{-1}), Pearl River (579 ± 389 m^3s^{-1}), Pascagoula River (723 ± 660 m^3s^{-1}), and Mobile River (1361 ± 240 m^3s^{-1}), respectively. Based on the information provided on the Mississippi River Flood Control website (https://www.mvn.usace.army.mil/Missions/Mississippi-River-Flood-Control/Bonnet-Carre-Spillway-Overview/Spillway-Operation-Information/) of the US Army Corps of Engineers, the Bonnet Carré Spillway connected to Lake Pontchartrain was opened during spring 2018 from 8th March 2018 to 30th March 2018. Additionally, the spillway was again opened two separate periods in 2019, from 27th February 2019 to 11th April 2019 (Winter 2019 through Spring 2019) and from 10th May 2019 to 27th July 2019 (Spring 2019 through Summer 2019).

In all six watersheds, the average daily precipitation was higher during both summers and was 7.04 mm in 2018 and 7.20 mm in 2019, while average precipitation was lower during spring 2018 at 4.16 mm. Similarly, the average precipitation of the six watersheds during winter 2018 was 5.20 mm (Table 1). Among six watersheds bordering the study area, the Mississippi Coastal watershed had the highest precipitation during summer 2018 and 2019 and was 7.83 ± 7.55 mm and 7.66 ± 8.89 mm and the lowest was in North Lake Ponchartrain Watershed and was 6.24 ± 5.64 mm and 7.14 ± 9.04 mm (Fig. 2). Although the precipitation was higher during both 2018 and 2019 summers compared to spring and winter 2018, summer river discharge during both 2018 and 2019 was generally lower, which may be due to stronger evapotranspiration in summer (Milliman, 2001).

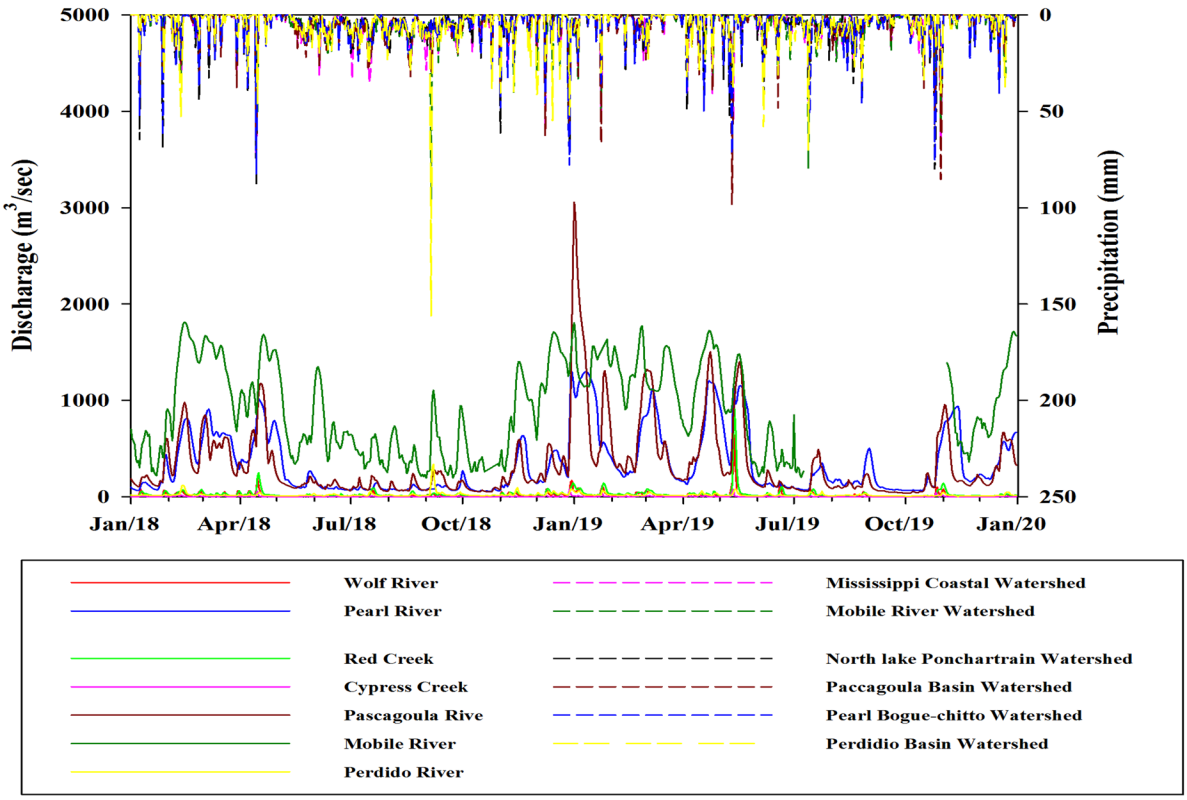

Fig. 2 The precipitation (dotted lines) in six watersheds and corresponding water discharge through the seven rivers/creeks (solid lines) bordering Western Mississippi Sound

Seasonal variation in physico-chemical parameters, trace elements, nutrients, and suspended particulate matter

Water depth, Secchi depth, and water quality parameters including surface water temperature and salinity are summarized in Table 2 and SI Fig. 1. The results suggest significantly ($p < 0.05$) higher surface water salinity during both the summer and winter of 2018 compared to the summer of 2019 (Table 2, SI Fig. 3). On the other hand, significantly higher but similar surface water temperature was observed during both summers (2018 and 2019) compared to the spring of 2018. Significantly lower surface water temperature was observed during winter 2018.

The average concentrations of Cu, Pb, Zn, U, and Ca in the study area were significantly higher ($p < 0.05$) during winter 2018 than the rest of the study period (Table 2, Fig. 3, SI. Fig. 2). Specifically, higher concentrations of Pb (224 %), Cu (211 %), Zn (2400 %), and Ca (240 %) were observed during the winter of 2018 compared to the summer of 2019. On the other hand, the concentration of As was significantly higher ($p < 0.05$) during summer 2018, and the concentration of Mn was higher during summer 2019 than other sampling seasons. Conversely, the average concentrations of dissolved As, Cu, Zn, and Ca were significantly lower ($p < 0.05$) during summer 2019 than the other periods. Similarly, the average concentrations of Mn and Pb were lowest during summer 2018, while for U, significantly lower average concentrations ($p < 0.05$) were observed during spring 2018 compared to the rest of the study period.

The average concentration of all the dissolved nutrients except NO_2^- was high during the summer of 2019 and low during winter (Table 2, Fig. 3, SI. Fig. 2). Conversely, the average concentration of NO_2^- was significantly higher ($p < 0.05$) during spring and was lowest during summer 2018. The concentration of PO_4^{3-} was also significantly higher ($p < 0.05$) during both summers

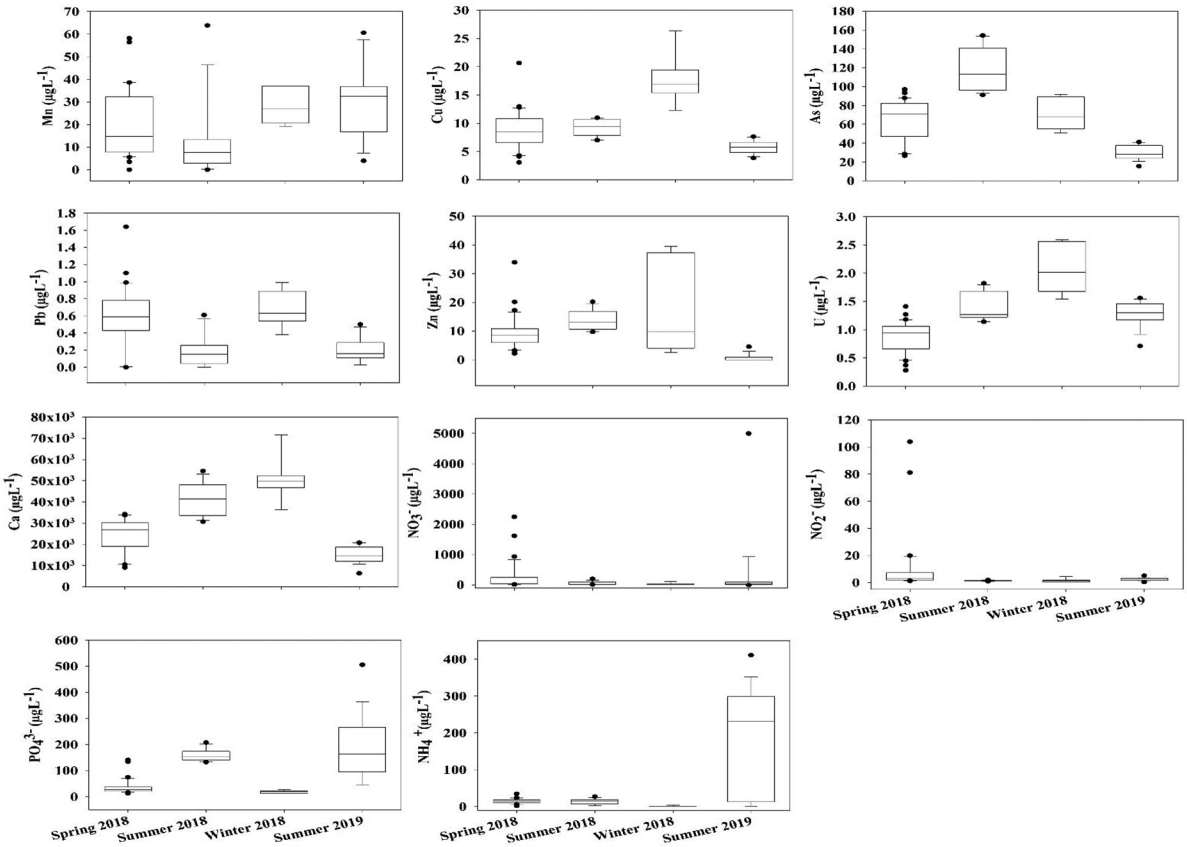

Fig. 3 Seasonal variation in concentration of trace elements, calcium, and nutrients in the study location following spring 2018 ($n = 31$), summer 2018 ($n = 14$), winter 2018 ($n = 7$), and summer 2019 ($n = 18$). "n" denotes the number of samples

(2018 and 2019), while NH_4^+ concentration was similar during the spring and summer of 2018. Mainly, the concentrations of both PO_4^{3-} and NH_4^+ were higher (> 800 %) during both summers than the winter of 2018.

Significantly higher SPM and SPOM ($p < 0.05$) during winter, significantly lower ($p < 0.05$) SPM and SPIM during summer 2019, and lower SPOM were observed during spring (Table 2, SI. Figs. 1 and 3). The amount of SPIM was reasonably higher during summer 2018 (SI Fig. 1). Additionally, SPOM was similar during both summers (2018 and 2019).

Seasonal variation of carbonate system parameters

The carbonate system parameters showed a strong seasonal trend in their distribution in the water column of the study area. The TA, pH, CO_3^{2-}, Ω_{Ca}, and Ω_{Ar} showed nearly a similar seasonal trend with an overall increase from spring 2018 to summer 2018, then decreased during winter 2018, and again increased during summer 2019 (Fig. 4, Table 3). Conversely, the DIC concentrations showed an increase from spring 2018 to summer 2018, then gradually decreased from winter 2018 through summer 2019. Average HCO_3^- gradually increased from spring 2018 through summer 2018 until winter 2018, then decreased during summer 2019. Furthermore, both TA, DIC, and HCO_3^- increased from the surface to bottom waters over the oyster bed during all seasons. The pH, CO_3^-, Ω_{Ca}, $\Omega_{Ar,}$ TA, DIC, and HCO_3^- showed a gradual decrease from the surface to bottom waters during all seasons. However, they were lower during the summer months (2018 and 2019). Compared to other seasons, the highest average values of both TA and DIC were observed during summer 2018. Equivalently, the average amount

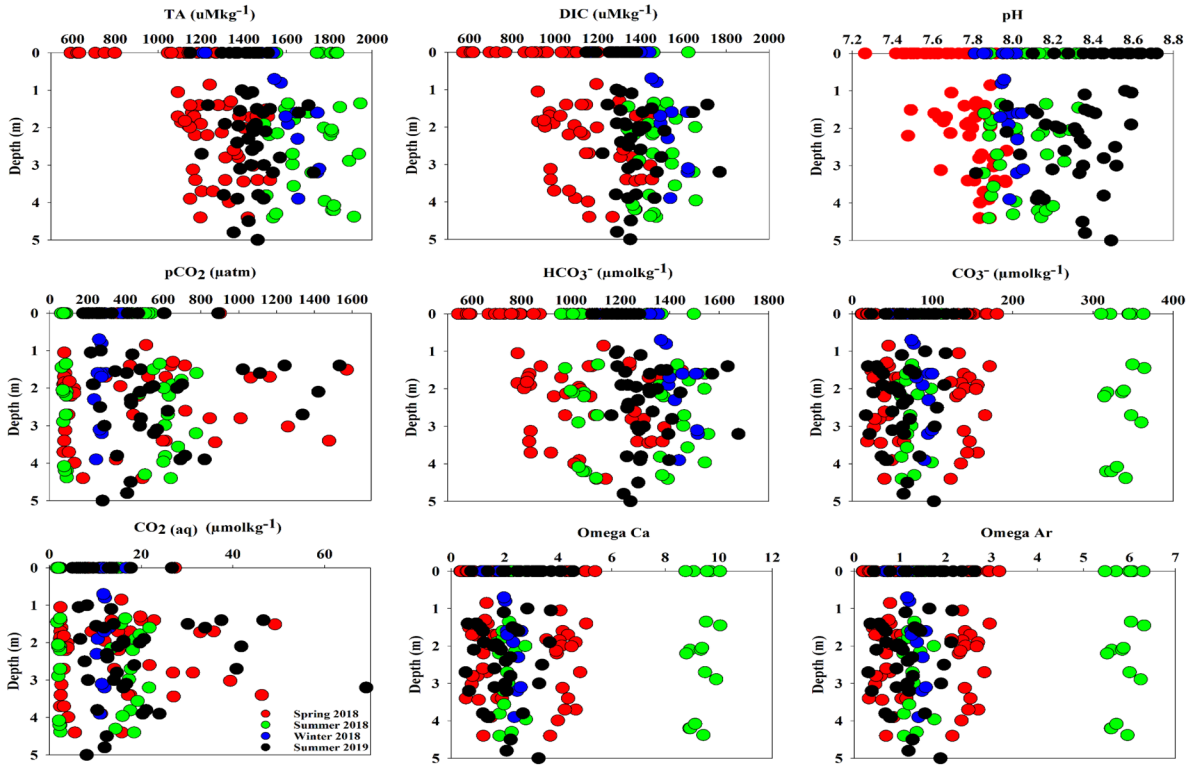

Fig. 4 Depth wise seasonal variation in ocean acidification parameters in the study location following spring 2018 (*n*, surface = 30; middle = 20; bottom = 22), summer 2018 (*n*, surface = 14; middle = 14; bottom = 14), winter 2018 (*n*, surface = 6; middle = 6; bottom = 6), and summer 2019 (*n*, surface = 17; middle = 17; bottom = 17). "*n*" denotes the number of samples

of HCO_3^- was lower during spring and higher during both summers (2018 and 2019). The pH during both spring and winter was lower compared to both summer (2019 and 2018) months. The average pCO_2 and CO_2 (aq) concentrations had a similar seasonal trend in the water column as they both are related to Henry's constant (K_H), which is a function of temperature and salinity. The carbonate system parameters for the surface waters also followed the above-mentioned trend (Table 3, SI Fig. 4).

Seasonal variation of organic matter and optical properties

The amount of DOC was significantly higher ($p < 0.05$, 4.84 ± 0.67 mg L^{-1}) during summer 2019 and was significantly lower ($p < 0.05$) during summer 2018 (3.56 ± 0.51 mgL^{-1}). Additionally, DOC concentrations showed a significant increase ($p < 0.05$) from summer 2018 to summer 2019 (Table 2, Fig. 5, SI. Fig. 6).

The PARAFAC modeling has resulted in three distinct compositions, C1 (Ex/Em < 250–310 nm/412 nm), C2 (Ex/Em 260–360 nm/486 nm), and C3 (Ex/Em < 250–280 nm/342 nm) (SI Fig. 5). Among the three components, two of them (C1 and C2) were terrestrial humic-like components that have been commonly identified in the near-shore marine ecosystems (Sankar et al., 2020, 2019a, b; Yamashita et al., 2010; Yu et al., 2015). The third component (C3) was a protein-like component that is often used to represent a freshly produced, biologically labile DOM of autochthonous origin (from algae and microbes), and it has been commonly found in cropland runoff, wastewater, and industrial effluents (Sankar et al., 2019a; Singh et al., 2017; Yu et al., 2015). The component C1 was found to be most abundant and followed by C2 and C3 in all sampling seasons (Table 2, Fig. 5, SI. Fig. 6). When the four seasons are compared, Terrestrial humic-like compositions C1 and C2 exhibited relatively similar seasonal variation. The C1 and C2 during both summer (11 %, 33 %) and spring (12 %,

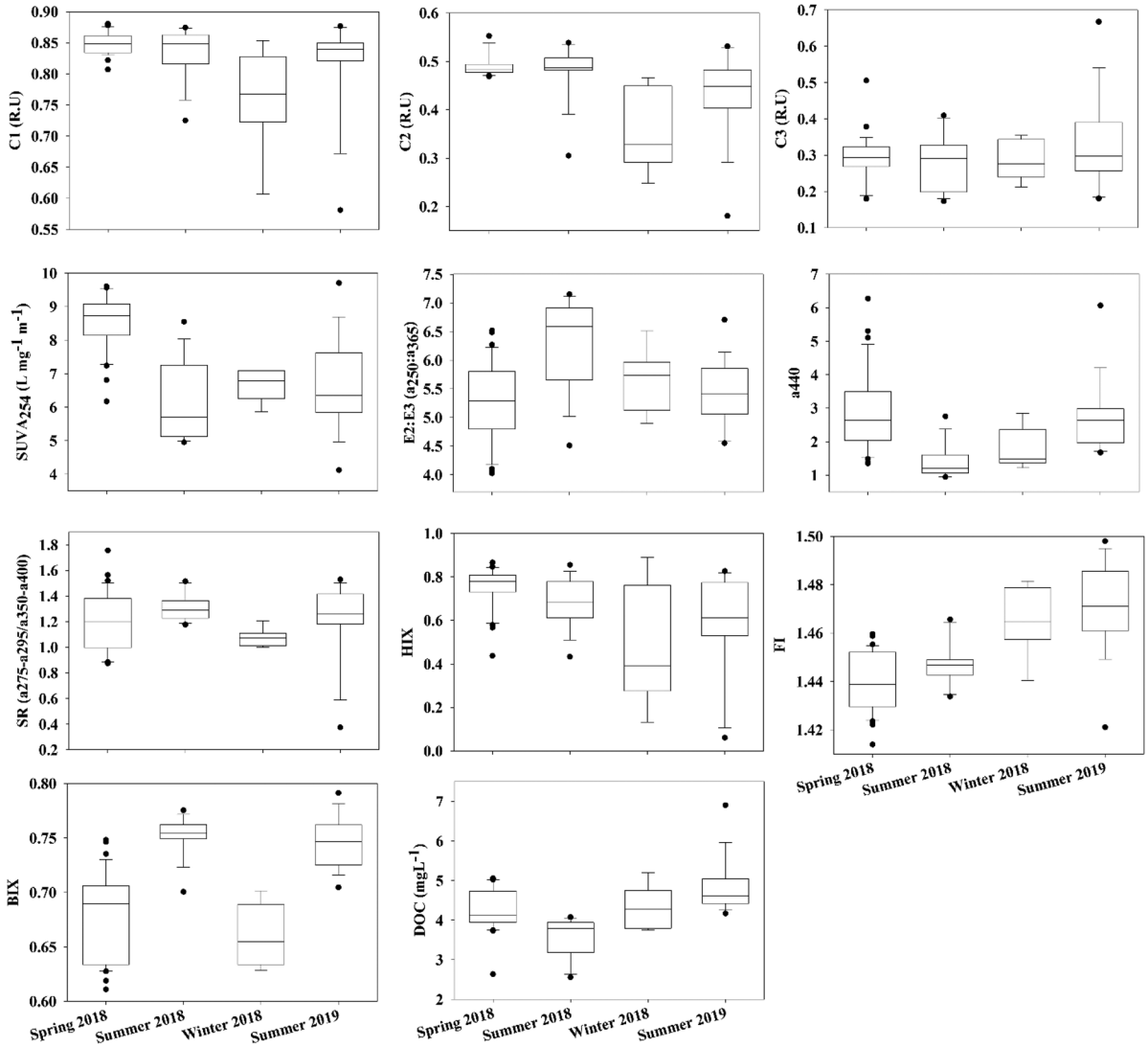

Fig. 5 Seasonal variation of PARAFAC components, absorption ($SUVA_{254}$, a440, E2:E3, SR), fluorescence indices (HIX, FI, BIX), and concentration of DOC in the surface waters over the study location in west Mississippi Sound following spring 2018 ($n=31$), summer 2018 ($n=14$), winter 2018 ($n=7$), and summer 2019 ($n=18$) sampling events. "n" denotes the number of samples

36 %) were significantly higher ($p<0.05$) than that during winter. Conversely, the concentration of protein-like component C3 was significantly lower during spring, summer, and winter of 2018 than during summer 2019.

Both UV and fluorescence indices expressed significant ($p<0.05$) seasonal control over the study area (Table 2, Fig. 5, and SI Fig. 6). The values of FI were always less than 1.5 and exhibited an increase from spring to summer 2019. Although BIX values were below one (< 1) during all seasons, its values were similar and significantly higher ($p<0.05$) during both summers (2018 and 2019) than during spring and winter. The HIX values were significantly lower ($p<0.05$) during winter and summer 2019 compared to both spring and summer 2018. Similarly, the $SUVA_{254}$ values were significantly lower but similar during winter 2018 and summer 2019 than spring 2018. Furthermore, values of $SUVA_{254}$ were significantly lower during summer 2018 and higher ($p<0.05$) during spring 2018 compared to

other seasons. Compared to other seasons, the SR values were significantly lower ($p<0.05$) during winter 2018, while E2:E3 ratios were significantly higher ($p<0.05$) during summer 2018. The *a*440 indices were similar and significantly higher ($p<0.05$) during spring 2018 and summer 2019 compared to summer and winter of 2018. Additionally, the *a*440 values showed a significant increase ($p<0.05$) from summer 2018 to summer 2019.

Multivariate spearman correlation for DOM optical indices showed a significant strong positive correlation between terrestrial humic-like components C1 and C2 ($p<0.05$; $r=0.79$), while both showed significant negative correlations against the protein-like component C3 ($p<0.05$; $r=-0.27$, $r=-0.42$). FI had a significant negative correlation against both terrestrial humic-like components ($p<0.05$; $r=-0.25$, $r=-0.31$). $SUVA_{254}$ had a significant positive correlation with one of the terrestrial humic-like compositions (C2) but a significant negative correlation with FI (Table 4). FI, BIX, and *a*440 showed significant negative correlation against HIX ($p<0.05$; $r=-0.24$, $r=-0.42$, $r=-0.42$). BIX showed a significant negative correlation with $SUVA_{254}$ ($p<0.05$; -0.52) and had a significant positive correlation against *a*440 ($p<0.05$; $r=0.62$). The E2:E3 ratio had significant negative correlations against $SUVA_{254}$ and *a*440 ($p<0.05$; $r=-0.37$, $r=-0.35$). Similarly, *a*440 also had a significant negative correlation against SR ($p<0.05$; $r=-0.37$).

Salinity versus dissolved constituents

There is strong seasonal control in the distribution of dissolved constituents along the entire salinity range. The salinity in the study area had a significant ($p<0.05$) positive correlation with trace elements including As ($r=0.93$), Cu ($r=0.46$), U ($r=0.61$), Ca ($r=0.92$), and Zn ($r=0.56$), while Mn ($r=-0.17$) and Pb ($r=-0.18$) had a nonsignificant ($p>0.05$) negative correlation with salinity (Fig. 6). Although the nutrients including NO_3^-, NO_2^-, PO_4^{3-}, and NH_4^+ had a negative relationship with salinity, only the relationship of NH_4^+ ($r=-0.47$) was significant ($p<0.05$) (Fig. 7). Conversely, for nutrients such as NO_3^- ($r=-0.17$), NO_2^- ($r=-0.07$), and PO_4^{3-} ($r=-0.01$), a nonsignificant relationship with salinity was observed (Fig. 6). Additional figures (SI. Figs. 7 and 8) were also created for NO_2^-, NO_3^-, and NH_4^+ by removing a few extreme values and by adding *Y*-axis breaks on the same figure (Fig. 6) to highlight the distribution of the sample points. Particularly, salinity had significant ($p<0.05$) positive correlations against SPM ($r=0.87$), SPIM ($r=0.83$), and SPOM ($r=0.34$) (Fig. 8). Most of the carbonate system parameters had significant ($p<0.05$) positive relationship with salinity except pH, pCO_2, and $CO_{2\,(aq)}$ (Fig. 9).

The DOM compositions showed a nonsignificant ($p>0.05$) association with salinity (Fig. 7). One of the terrestrial humic-like compositions C1 ($r=-0.06$) and tryptophan-like or protein-like component C3 ($r=-0.19$) showed a negative relationship with salinity, while the other terrestrial humic-like composition C2 showed no relationship with salinity. DOM optical indices including E2:E3 ($r=0.29$), SR ($r=0.29$), and BIX ($r=0.14$) showed positive, while $SUVA_{254}$ ($r=-0.40$), *a*440 ($r=-0.42$), HIX ($r=-0.13$), and FI ($r=-0.14$) had negative relationship against salinity; the relationship was significant ($p<0.05$) only for $SUVA_{254}$, E2:E3, *a*440, and SR. Similarly, the DOC also had significant negative relationship with salinity ($p<0.05$, $r=-0.62$).

Results of principal component analysis

The PCA biplot was generated by incorporating the concentrations of trace elements, nutrients, DOC, PARAFAC components, DOM optical indices, SPM data, carbonate system parameters (pH, DIC, TA), salinity, and water temperature collected during the four seasons as PCA loadings (Fig. 10). The rest of the derived carbonate system parameters were not included into the PCA as their values depend upon both TA and DIC. The biplot containing two principal components (PC) as indicated by PC1 (25.9%) and PC2 (21.2%) together explained 47.1% of the total variance of the input data. The PC1 axis separates the loadings of organic matter from inorganic components. Additionally, the terrestrial humic-like components including C1 and C2 had negative loadings and protein-like component C3 had a positive loading on PC2. The terrestrial humic-like compositions have a close association with $SUVA_{254}$ and HIX and were on the negative PC2

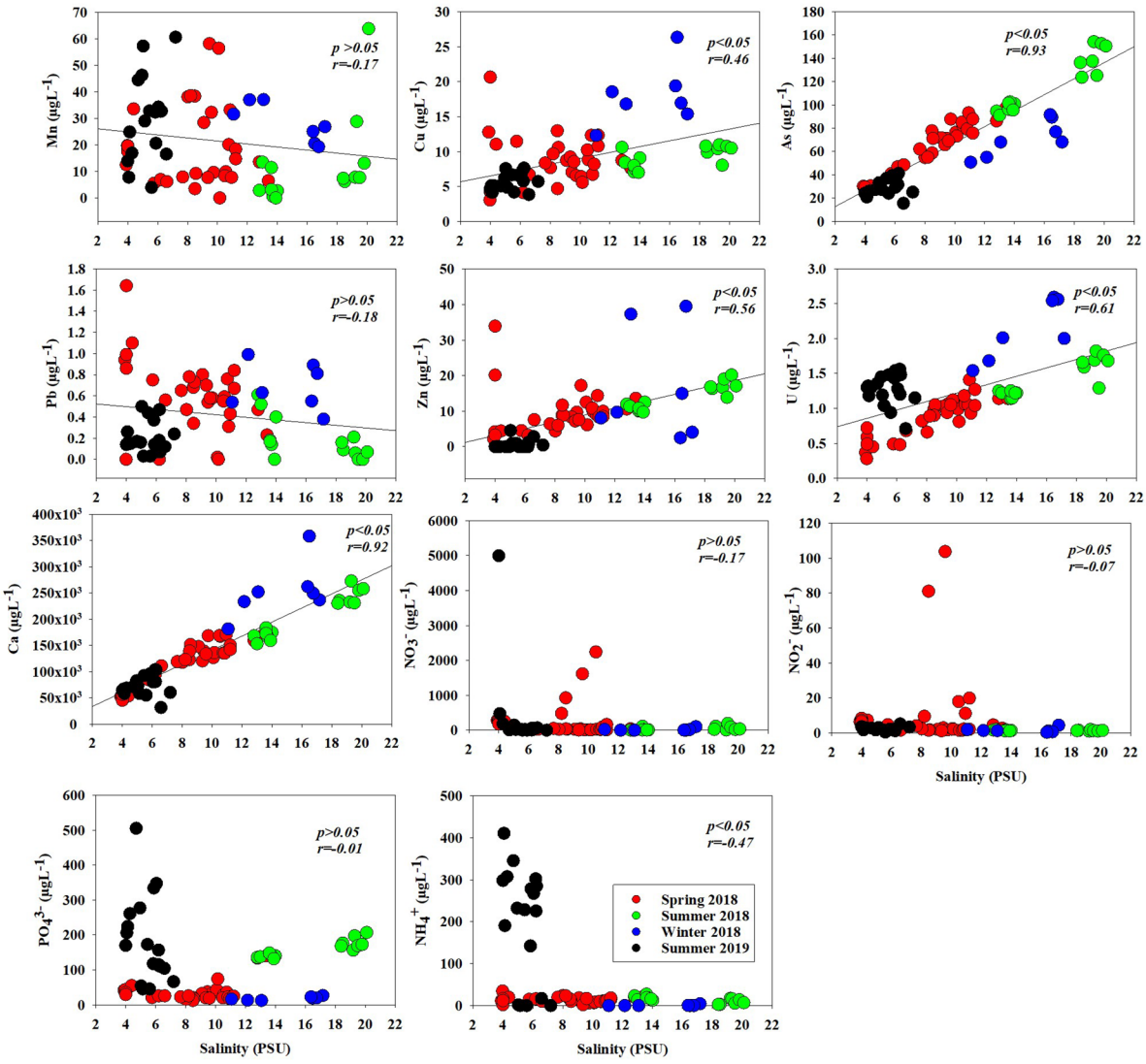

Fig. 6 Relationship of trace elements and nutrients with salinity in the surface waters of the study location in west Mississippi Sound

axis, while the tryptophan-like or protein-like component and FI and BIX were associated along the positive PC2 axis. The salinity showed a positive relation with SPM, SPIM, As, Ca, Cu, and Zn and were located on the negative PC2 axis. Similarly, the TA, DIC, pH, and temperature were positively related and were located on the positive PC2 axis. In the same way, SPOM, U, SR, and E2:E3 were also directly related to the positive side of the PC1 axis. The scores of the samples collected during 2018 (spring, summer, and winter) were spread across the PC1 axis, while the scores of the samples collected during 2019 (summer) were located on the positive side of the PC2 axis.

PCA analysis suggests correlation between the trace elements, Ca, and SPM, particularly during winter 2018 season. Therefore, a detailed analysis of the winter 2018 subset using Spearman's rank correlation was performed, which revealed that both Cu, Ca, As, Pb, and U had moderate to

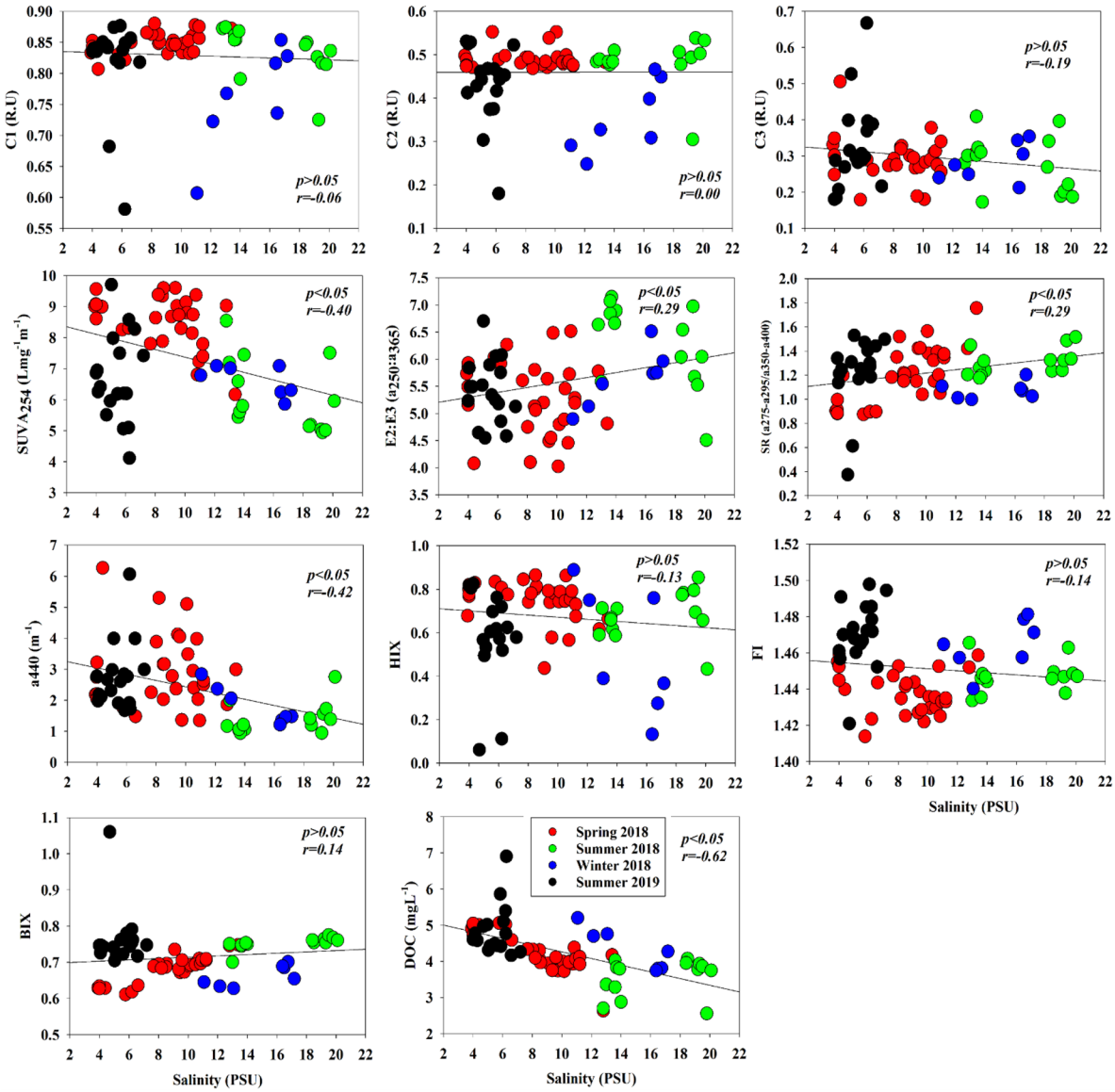

Fig. 7 Relationship of the DOM composition, optical indices, and the concentration of DOC with salinity in the surface waters of the study location in west Mississippi Sound

strong positive association with SPM and SPIM. Among them, only Cu, As, Ca, and U had strongly to moderately positive association and Zn had weakly negative association with SPOM. Additionally, the SPOM was significantly correlated ($p<0.05$) with Cu and Ca. On the other hand, Mn had a negative correlation with SPM, SPIM, SPOM, and all other elements. Among them, only U had significant relationship with Mn. A significant strong, positive correlation between SPM and SPIM was also identified (SI. Table 2).

Discussion

Seasonal change in water quality over the oyster reef

The findings in this study suggest that precipitation in the watersheds and discharge of the rivers have significant control over the seasonal changes in water quality over the oyster reef in terms of mobilization of elements and alteration of biogeochemical parameters. The presence

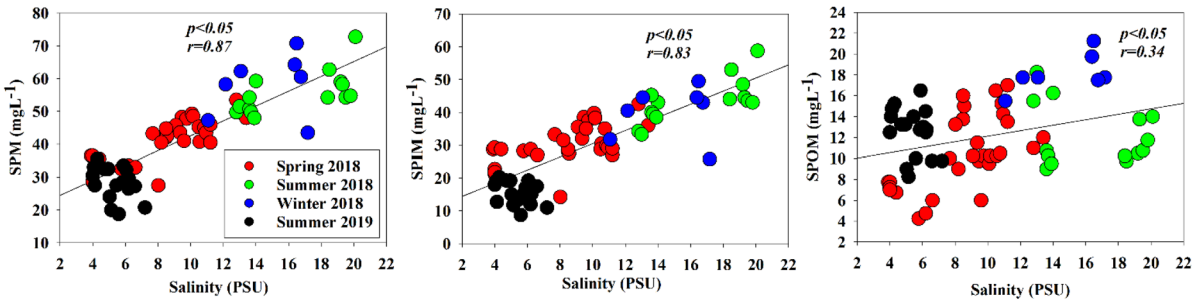

Fig. 8 Relationship of the SPM, SPIM, and SPOM with salinity in the surface waters of the study location in west Mississippi Sound

of higher amounts of trace elements (e.g., Cu, Pb, Zn, U, and As), Ca, and particulate matter (measured by SPM, SPIM, and SPOM) during winter, spring, and summer of 2018 is attributed to relatively higher discharge during these seasons compared to summer of 2019. The distribution of trace elements through their association with SPM in coastal waters has been well established (Balls, 1990; van der Sloot Hans et al., 1990; Jokinen et al., 2020; Koukina & Lobus, 2018; Kuwabara et al., 1989; Regnier & Wollast, 1993; Turner & Millward, 2000). Higher discharge of rivers flowing through the six watersheds along with the Mississippi River water diverted

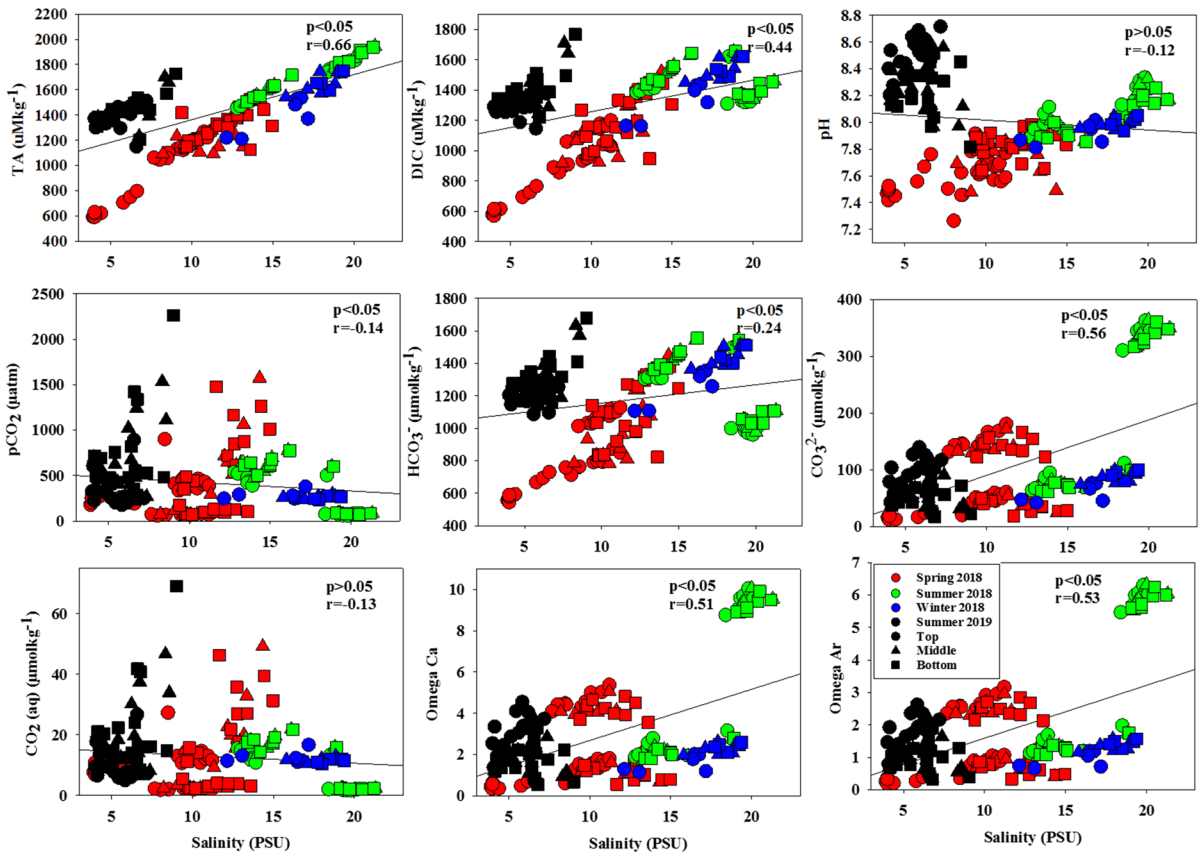

Fig. 9 Relationship of the ocean acidification parameters with salinity in the surface, middle, and bottom waters of the study location in west Mississippi Sound

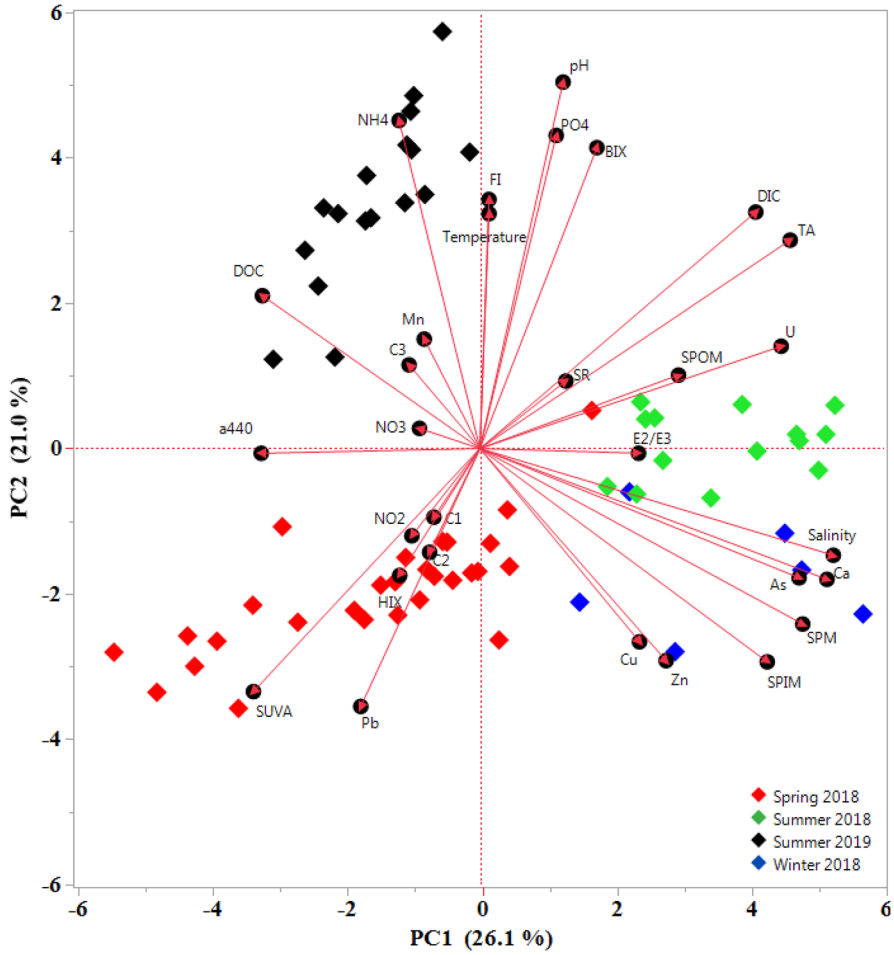

Fig. 10 Principal component analysis (PCA) biplot for surface water composition of the study location in west Mississippi Sound following spring 2018 ($n=28$), summer 2018 ($n=14$), winter 2018 ($n=6$), and summer 2019 ($n=18$). The seasonal sampling events were represented by distinct colors. "n" denotes the number of samples

through the Bonnet Carré spillway opening delivered a higher amount of dissolved trace elements associated with SPM over the waters of Western Mississippi Sound. Similar observations on higher concentration of trace elements during the times of higher discharge into the adjacent bays and rivers including Mobile Bay, Weeks Bay, Mississippi River, and Pearl River have also been reported (Lafabrie et al., 2011; Sankar et al., 2019a; Stolpe et al., 2010). Salinity was higher during summer and winter seasons of 2018 compared to the spring 2018 and summer of 2019. This observation again reinforces the interpretation that freshwater influx during spring 2018 and higher precipitation during summer of 2019 resulted in higher delivery of both dissolved material and suspended particles into the sound. Previous studies suggested multiple sources for the fluxes of the above-mentioned trace elements including Mn delivered along the coastal waters of the northern Gulf of Mexico and regions adjacent to the study area. The sources of trace elements include effluents from chemical industrial plants in the urbanized areas which is between 6.06 and 10.6% of total area (Lafabrie et al., 2011; Sankar et al., 2019a; Zielinski et al., 2007), reductive dissolution of sea bottom sediments along with decomposing organic matter (Joung & Shiller, 2016; Sankar et al., 2019a; Slowey & Hood, 1971), desorption from the agricultural soil due to the nitrification and soil acidification from the application of ammonium fertilizer (Sankar et al., 2019a), fertilizers such as basic slag (Sankar et al., 2019a), and arsenical pesticides and herbicides applied to the croplands years ago (Sankar et al., 2019a).

During both summers (2018 and 2019), the average discharge was comparatively lower, yet the amount of precipitation was higher compared to other seasons in the study area. The greater concentrations of NO_3^-, PO_4^{3-}, NH_4^+, and Mn during summer 2019

Table 1 The seasonal average precipitation in six watersheds and corresponding seasonal average discharge through the seven rivers/creeks bordering west Mississippi Sound

	Spring 2018	Summer 2018	Winter 2018	Summer 2019
Watershed	***Precipitation (mm)***			
Mississippi Coastal	4.51 ± 10.51	7.83 ± 7.55	4.92 ± 10.50	7.66 ± 8.89
Mobile River Basin	4.00 ± 7.86	7.08 ± 5.51	5.15 ± 10.85	7.13 ± 10.57
North Lake Ponchartrain	4.08 ± 11.2	6.24 ± 5.64	5.18 ± 11.48	7.14 ± 9.04
Pascagoula Basin	4.89 ± 10.4	7.70 ± 7.28	5.37 ± 12.27	7.12 ± 8.72
Pearl Bogue-Chitto	4.14 ± 10.5	6.59 ± 5.92	5.57 ± 12.50	6.88 ± 9.11
Perdidio Basin	3.35 ± 6.82	6.79 ± 6.29	5.04 ± 11.09	7.25 ± 11.0
Average of 6 watersheds	***4.16***	***7.04***	***5.20***	***7.20***
River/creek	***Discharge m^3s^{-1}***			
Mobile River	1106 ± 413	540 ± 258	1361 ± 240	631 ± 393
Perdido River	15.7 ± 6.32	15.7 ± 7.82	28.9 ± 15.9	17.8 ± 12.6
Pascagoula River	410 ± 285	108 ± 44.3	723 ± 659	146 ± 95.8
Cypress Creek	3.41 ± 6.45	1.50 ± 1.48	5.29 ± 9.45	1.20 ± 1.45
Red Creek	28.7 ± 37.3	18.3 ± 16.6	42.0 ± 30.7	20.3 ± 18.3
Pearl River	497 ± 268	88.8 ± 24.4	579 ± 388	301 ± 3105
Wolf River	17.6 ± 26.1	7.97 ± 10.0	29.8 ± 29.40	13.0 ± 19
Average of 7 rivers/creeks	***297***	***111***	***395***	***161***

compared to other seasons of 2018 may be attributed to precipitation-mediated leaching combined with reduced river discharge. Higher precipitation in the region might have accelerated the leaching of phosphate and nitrate-based fertilizers being applied to the agricultural areas (0.83–12.8%) and from the dissolution of waste materials present in the feedlots of pastures (3.54–12.2%) and rangeland (17.3–26.1%) areas of these watersheds. Consequently, a high amount of dissolved nutrients from agricultural, pastoral, and rangeland areas of six watersheds entered the river system during the events of heavy precipitation and eventually ended up in the sound waters during summer months. Furthermore, Bonnet Carré Spillway opening and freshwater discharge during the summer of 2019 and late spring of 2018 supplemented the dilutional effects of trace elements in the study area during summer.

Seasonal variability and elevated alkalinity at shallower depths were well documented over the northern Gulf of Mexico similar to Chesapeake Bay (Cai et al., 2017; Renforth & Henderson, 2017; Yang et al., 2015). The findings in this study also suggested seasonal variation along with significant but weak positive correlation between TA ($p<0.05$, $r=0.30$), DIC ($p<0.05$, $r=0.33$), and HCO_3^- ($p<0.05$, $r=0.30$) with the depth of the waters (0–6 m) over the oyster reef. Studies conducted in the northwestern Gulf of Mexico and Louisiana Shelf suggest that the temporal changes in the mixing of seawater and fresh waters along with remineralization and respiration of organic matter could be the main factor for such seasonal and depth-wise variation in alkalinity (Hu et al., 2015; Wanninkhof et al., 2015; Yang et al., 2015). Similarly, the river discharge data collected for the present study also revealed a significant seasonal variation signifying the temporal changes in freshwater input. pH, CO_3^{2-}, Ω_{ca}, and Ω_{Ar} showed a decreasing trend with depth during the summer seasons (2018 and 2019), suggesting organic matter remineralization and subsequent lowering of acidity. Additionally, higher precipitation, along with higher pH, CO_3^{2-}, Ω_{Ca}, and Ω_{Ar} during both summers, suggests a higher rate of chemical weathering of calcareous rocks of the Gulf Coast deposits in the watersheds and hence higher input of both Ca and CO_3^{2-} into the sound (Renforth & Henderson, 2017). Carbonate weathering and input from inland areas can increase the pH, Ω_{Ca}, and Ω_{Ar} in the waters of the Western Mississippi Sound during both summers, as indicated by significant positive relation of water temperature against pH ($p<0.05$, $r=0.24$), Ω_{Ca} ($p<0.05$, $r=1.00$), and Ω_{Ar} ($p<0.05$, $r=1$), again manifests the above observation. The seasonal depth-wise difference in change of pH, CO_3^{2-}, Ω_{Ca}, and Ω_{Ar} could also be due to the seasonally regulated higher input of alkaline load through the rivers and its strong buffering capacity over the entire salinity

Table 2 The seasonal averages of surface water quality parameters, dissolved constituents, DOM optical properties, and depth to the bottom of the study area

Variable	*Spring 2018*	*Summer 2018*	*Winter 2018*	*Summer 2019*
Mn (μgL^{-1})	19.4 ± 15.0	12.0 ± 16.6	28.2 ± 7.26	30.0 ± 15.5
As (μgL^{-1})	63.7 ± 21.9	118 ± 23.8*	71.4 ± 15.70	29.8 ± 7.36
Cu (μgL^{-1})	8.72 ± 3 .51	9.21 ± 1.50	17.9 ± 4.36*	5.76 ± 1.21
Pb (μgL^{-1})	0.60 ± 0.35	0.19 ± 0.19	0.68 ± 0.22*	0.21 ± 0.15
Zn (μgL^{-1})	9.47 ± 6.09	14.0 ± 3.58	16.5 ± 15.46*	0.66 ± 1.22
U (μgL^{-1})	0.87 ± 0.28	1.42 ± 0.26	2.13 ± 0.44*	1.27 ± 0.22
Ca (μgL^{-1})	1,210,123 ± 39,883	206,824 ± 42,005	253,441 ± 53,211*	74,463 ± 19,133
NO_3^- (μgL^{-1})	242 ± 494	47.7 ± 57.2	23.4 ± 36.1	341 ± 1167
PO_4^{3-} (μgL^{-1})	36.5 ± 29.7	159 ± 23.2*	18.5 ± 5.11	184 ± 123*
NO_2^-(μgL − 1)	10.6 ± 22.5*	1.38 ± 0.29	1.51 ± 1.34	2.27 ± 1.06
NH_4^+ (μgL^{-1})	14.1 ± 6.8	13.8 ± 7.26	0.64 ± 1.55	196 ± 135*
SPM (mgL^{-1})	40.9 ± 6.9	55.6 ± 6.50	58.1 ± 9.59*	28.2 ± 4.85*
SPIM (mgL^{-1})	30.4 ± 5.9	43.5 ± 6.77	39.9 ± 8.28	15.6 ± 3.39*
SPOM (mgL^{-1})	10.4 ± 3.54	12.1 ± 2.88	18.18 ± 1.83*	12.5 ± 2.30
Water depth (m)	3.08 ± 0.76	3.68 ± 0.64	2.69 ± 0.89	3.45 ± 0.96
Temperature (C°)	24.6 ± 4.36	29.7 ± 0.88	12.52 ± 0.29*	29.5 ± 0.92
Salinity (PSU)	8.62 ± 2.91	16.3 ± 3.03*	15.59 ± 2.08*	5.42 ± 0.94*
Secchi depth (cm)	72.3 ± 21.2	112 ± 43.7	155 ± 16.6	78.4 ± 54.7
DOC (mgL^{-1})	4.26 ± 0.54	3.56 ± 0.51*	4.33 ± 0.57	4.84 ± 0.67*
$SUVA_{254}$ (L mg^{-1} m^{-1})	8.55 ± 0.84*	6.11 ± 1.16	6.63 ± 0.49	6.69 ± 1.39
E2:E3	5.30 ± 0.69	6.30 ± 0.76*	5.65 ± 0.53	5.42 ± 0.57
a440 (m^{-1})	2.89 ± 1.18*	1.39 ± 0.50	1.83 ± 0.61	2.75 ± 1.07*
SR	1.20 ± 0.23	1.31 ± 0.11	1.07 ± 0.07*	1.22 ± 0.29
HIX	0.75 ± 0.10*	0.68 ± 0.11	0.51 ± 0.29	0.60 ± 0.22
FI	1.44 ± 0.01*	1.45 ± 0.01	1.46 ± 0.01	1.47 ± 0.02
BIX	0.68 ± 0.04	0.75 ± 0.02*	0.66 ± 0.03	0.76 ± 0.08*
C1 (R.U)	0.85 ± 0.02*	0.84 ± 0.04*	0.76 ± 0.08	0.82 ± 0.07
C2 (R.U)	0.49 ± 0.02*	0.48 ± 0.05*	0.36 ± 0.08	0.43 ± 0.09
C3 (R.U)	0.29 ± 0.06	0.28 ± 0.08	0.28 ± 0.05	0.33 ± 0.12*

The asterisk symbol "*" represents significant ($p < 0.05$) differences (increase or decrease)

range along the coastal region near Western Mississippi Sound (Cai et al., 2017). The values of Ω_{Ca} and Ω_{Ar} both measure of thermodynamic preference of the mineral $CaCO_3$ to form (> 1) or to dissolve (< 1), and calcifying organisms including oysters require Ω_{Ar} ratio above 1.0 (Feely et al., 2012). Our results indicate that majority of the Ω_{Ca} and Ω_{Ar} values were always greater than 1 during all seasons suggesting that the waters of the study region over the oyster reef are over the $CaCO_3$ saturation state. The present study demonstrated slight seasonal variation of pCO_2 with comparatively higher levels of pCO_2 during both summers compared to the rest of the seasons, suggesting seasonal variability of wind speed and air-sea gas exchange favoring seasonal CO_2 mixing. The significantly ($p < 0.05$) higher amount of CO_2 during winter 2018 compared to other seasons suggests a lower amount of CO_2 uptake by phytoplankton during winter 2018. A significantly higher ($p < 0.05$) amount of PO_4^{3-} during both summers could increase the phytoplankton activity or algal bloom and hence higher CO_2 uptake than winter and spring.

The two terrestrial humic-like compositions (C1 and C2) showed similar seasonal variation, which suggests their similar source of origin as forests (24.54–46.50% of the total watershed area) and wetlands (19.8 to 31.1% of the total watershed area) and

Table 3 The seasonal averages of carbonate system parameters at the surface, middle, and bottom depths in the study area

Variable	*Depth*	*Spring 2018*	*Summer 2018*	*Winter 2018*	*Summer 2019*
TA (µMkg^{-1})	Top	1035 ± 273	1653 ± 155*	1392 ± 148	1389 ± 83.9
	Middle	1247 ± 136	1708 ± 139	1642 ± 85.1	1444 ± 108
	Bottom	1311 ± 113	1727 ± 146	1679 ± 66.4	1447 ± 110
DIC (µmkg^{-1})	Top	948 ± 243*	1395 ± 79.4	1320 ± 128	1293 ± 58.0
	Middle	1147 ± 187	1461 ± 104	1533 ± 72.5	1385 ± 121
	Bottom	1210 ± 1210	1481 ± 96.8	1560 ± 58.6	1401 ± 118
pH	Top	7.62 ± 0.16	8.11 ± 0.14*	7.91 ± 0.08	8.48 ± 0.17*
	Middle	7.76 ± 0.13	8.05 ± 0.16	7.99 ± 0.04	8.30 ± 0.19
	Bottom	7.86 ± 0.10	8.03 ± 0.14	8.00 ± 0.04	8.25 ± 0.19
pCO_2 (µatm)	Top	278 ± 197	301 ± 210	283 ± 49.2	337 ± 178
	Middle	425 ± 392	387 ± 286	264 ± 21.3	609 ± 379
	Bottom	497 ± 443	395 ± 287	258 ± 17.61	714 ± 498
HCO_3^- (µmolkg^{-1})	Top	867 ± 232*	1194 ± 187	1248 ± 114	1193 ± 53.7
	Middle	1049 ± 216	1264 ± 217	1435 ± 63.6	1303 ± 1263
	Bottom	1109 ± 191	1284 ± 207	1456 ± 52.7	1323 ± 114
CO_3^{2-} (µmolkg^{-1})	Top	71.9 ± 56.7	192 ± 132*	59.0 ± 15.8	89.8 ± 30.8
	Middle	84.0 ± 51.9	186 ± 136	85.6 ± 10.3	64.4 ± 28.7
	Bottom	85.9 ± 54.1	185 ± 135	92.0 ± 7.40	56.5 ± 24.4
CO_2 (aq) (µmolkg^{-1})	Top	9.10 ± 5.89	8.45 ± 5.97	12.7 ± 2.09*	9.97 ± 5.38
	Middle	13.1 ± 12.1	10.9 ± 8.14	11.73 ± 0.86	18.1 ± 11.5
	Bottom	15.4 ± 13.7	11.1 ± 8.16	11.36 ± 0.71	21.3 ± 15.1
Ω_{Ca}	Top	2.17 ± 1.72	5.44 ± 3.63*	1.58 ± 0.41	2.90 ± 1.00
	Middle	2.50 ± 1.56	5.21 ± 3.73	2.25 ± 0.27	2.06 ± 0.92
	Bottom	2.53 ± 1.60	5.19 ± 3.71	2.41 ± 0.19	1.81 ± 0.78
Ω_{Ar}	Top	1.26 ± 1.00	3.39 ± 2.30*	0.93 ± 0.25	1.67 ± 0.58
	Middle	1.46 ± 0.90	3.25 ± 2.36	1.34 ± 0.16	1.19 ± 0.53
	Bottom	1.49 ± 0.94	3.24 ± 2.36	1.44 ± 0.12	1.04 ± 0.45

The asterisk symbol "*" represents significant ($p < 0.05$) differences (increase or decrease)

their co-occurrence and transport. Moreover, studies showed that the forests, woody, and herbaceous wetlands in the watersheds can be a major source of terrestrial humic-like DOM composition present in the water bodies (Sankar et al., 2020, 2019a, b). Land use and land cover analysis of the six watersheds adjoining the study area also indicated that forests were predominant land cover class (total area 14,058 km^2) with significant coastal coverage of woody and herbaceous wetlands (total 9369 km^2), which could

Table 4 Multivariate Spearman correlation matrix of three parallel factor components/compositions and dissolved organic matter optical indices identified for the surface waters of west Mississippi Sound during spring 2018, summer 2018, winter 2018, and summer 2019

	C1	C2	C3	HIX	FI	BIX	SUVA	E2:E3	*a*440	SR
C1										
C2	***0.79***									
C3	***−0.27***	***−0.42***								
HIX	−0.05	0.15	−0.13							
FI	***−0.25***	***−0.31***	0.14	***−0.24***						
BIX	0.06	−0.02	0.03	***−0.42***	0.17					
$SUVA_{254}$	0.21	***0.26***	−0.03	0.11	***−0.32***	***−0.52***				
E2:E3	0.10	0.04	0.04	0.03	0.02	0.04	***−0.37***			
***a*440**	0.05	−0.04	−0.01	***−0.42***	−0.19	***0.62***	0.00	***−0.35***		
SR	0.03	0.12	0.01	0.14	0.18	0.06	−0.12	***−0.38***	***−0.37***	

The bold italics numbers represent significant ($p < 0.05$) relationships

serve as a persistent source of terrestrial humic-like DOM transported to Western Mississippi Sound. The presence of the significantly lower ($p < 0.05$) amount of terrestrial humic-like DOM in the Western Mississippi waters during winter could be due to its lesser supply compared to summer and spring. Similar observations were reported from a forested watershed in the Mid-Atlantic, piedmont region of MD, USA (Singh et al., 2014). Fairly higher amount of tryptophan-like or protein-like composition (C3) during summer 2019 compared to other seasons suggested relatively higher autochthonous production during summer 2019. The gradual increase of both DOC, a440, and FI values (< 1.5) from spring 2018 to summer 2019 suggested predominant terrestrial input. The persistence of lower BIX values (< 1) also reaffirms allochthonous DOM input. However, comparatively higher BIX values during summer seasons suggest relatively autochthonous production during summer seasons. Meanwhile, high average surface water temperature, comparatively higher amount of NO_3^-, and significantly higher ($p < 0.05$) concentration of PO_4^{3-} were also observed during both summers. Thus, a higher amount of nutrients along with ambient water temperature could enhance the amount of phytoplankton, thus resulting higher amount of algal derived, freshly produced, biologically labile autochthonous tryptophan-like or protein-like DOM composition during the summer season. Recurrence of intense algal blooms and hypoxia over the waters of the northern Gulf of Mexico during summer months as a result of ambient temperature and nutrient input has been widely reported (Rabalais et al., 2002; Sellner et al., 2003; Stumpf et al., 2003; Turner et al., 2006).

Seasonality in the mixing of dissolved and undissolved constituents

Calcium, TA, DIC, SPM, SPIM, SPOM, and most of the trace elements such as Cu, As, U, Zn, and DOC showed a conservative mixing behavior with a linear mixing trend against salinity of the waters of Western Mississippi Sound. Although the nutrients including PO_4^{3-}, NO_3^-, NO_2^-, and NH_4^+; cations such as Mn and Pb; most of the carbonate system parameters including pCO_2, CO_2 (aq), pH, HCO_3^-, CO_3^{2-}, Ω_{Ca}, and Ω_{Ar}; and DOM-PARAFAC compositions C1, C2, and C3 showed conservative mixing behavior, none of them had any specific enrichment or depletion trend along the mixing line. Similar observations for Mn, U, DOC, PO_4^{3-}, and NO_3^- were also identified near our study areas along the coast of Mississippi and Louisiana (Ho et al., 2019; Joung & Shiller, 2016). While comparing the seasonal mixing behavior, the summer 2019 samples are towards the lower salinity range compared to the samples collected during spring, summer, and winter of 2018 suggesting that higher precipitation and lower discharge, and low salinity during summer of 2019 might have influenced the mixing of the dissolved/undissolved constituents. Additionally, the sudden input of freshwater due to continued opening of the Bonnet Carré Spillway during 2019 summer caused lower salinity. The above finding also signifies the influence of local weather conditions, riverine input, and Bonnet Carré Spillway opening on salinity and mixing behavior in the Western Mississippi Sound. Additionally, the higher concentrations of Ca and the trace elements such as Cu, As, Pb, Zn, and U during the events of higher river discharge and low precipitation in spring and winter of 2018 could be the result of seasonal variations of the tributary mixing ratios as well as the change in redox chemistry within the river system. The trace element Mn showed no seasonal mixing behavior. However, its resemblance with the mixing on NH_4^+ suggested a seasonal change in redox conditions as well as variation in microbial Mn oxidation in the bottom waters of the sound. Similar observations were also identified in Weeks Bay, Alabama, as well as along the coast of Louisiana and these are adjacent to the study area (Joung & Shiller, 2016; Sankar et al., 2019a). The similarity in the seasonal distribution of As, Ca, SPM, and SPIM along their mixing line indicates their co-transport. Similarly, many of the sample points of both As and Ca were above the conservative mixing line implying that both As and Ca were released from SPM or colloidal particles upon mixing. Similar observations were made during the mixing experiments conducted along the Kona Coast of Hawaii (Johannesson et al., 2017). Additionally, Cu, Mn, As, Pb, Zn, Ca, and U during winter 2018 exhibited a bell-shaped distribution, with a maximum around salinity of 16, which also coincides with the SPM maximum, suggesting their peak transport during winter 2018. Similarly, their distribution during summer 2019 coincides with SPM minimum at a lower salinity range, suggesting

minimal transport of Cu, Mn, As, Pb, Zn, Ca, and U during summer 2019. The Bonnet Carré Spillway discharge produced a distinct increase in the concentrations of PO_4^{3-} and NH_4^+ in the sound during 2019. This suggests that though the discharge was low, the higher precipitation in the watersheds during both summers might have caused the increased delivery of PO_4^{3-} from fertilizers applied to agricultural areas of the watersheds into the sound. Additionally, the frequent freshwater input from the Bonnet Carré Spillway during summer months might have also delivered higher amount of dissolved PO_4^{3-}, which might have also influenced its concentration in the study area. Although the present study coincided with two of the spillway openings (spring 2018 and summer 2019), only the summer 2019 spillway opening had a detectable impact on our nutrient concentrations, especially on PO_4^{3-} and NH_4^+. This also implies that prevailing natural and anthropogenic conditions at the time of spillway openings could have influenced nutrient dynamics of this region. Parra et al. (2020) have also reported similar observations. Similarly, the carbonate system parameters such as TA, DIC, HCO_3^-, and pH had most of their summer 2018 and 2019 data points above the conservative mixing line suggesting inland weathering and dissolution of carbonate rocks and corresponding increase in pH in the sound waters as the result of higher amount of precipitation events during summer seasons. The close similarity in seasonal mixing trends of CO_3^{2-}, Ω_{Ca}, and Ω_{Ar} illustrates their interrelationship in the waters of the study area.

Reappraisal of water quality and coastal acidification based on principal component analysis

The PCA analysis of surface water quality data comprising of salinity, water temperature, concentrations of trace elements including a major element Ca, concentrations of nutrients including DOC, carbonate system parameters (TA, DIC, pH), DOM compositions, and its optical indices further show seasonally and hydrologically controlled changes in water chemistry over the oyster reef in the Western Mississippi Sound. The PC2 axis separates 2018 samples from 2019 suggesting the influence of seasonal rainfall, riverine discharge, and Bonnet Carré Spillway opening events on the water quality of the region. The close association of spring and winter 2018 samples scores along with $SUVA_{254}$, terrestrial humic-like compositions (C1 and C2), HIX, Pb, As, Cu, Zn, Ca, SPM, SPIM, and salinity suggests high aromatic character and similar source of origin, their co-transport as well as delivery into the Western Mississippi Sound during spring and winter of 2018. This substantiates our previous interpretation that higher river discharge during the spring and winter of 2018 brought a high amount of aromatic terrestrial humic-like DOM compositions from the inland forested and woody herbaceous wetland areas of the watersheds along with the high amount of Pb, As, Cu, Zn, and Ca adsorbed to SPM and SPIM from the agricultural areas. Additionally, higher discharge and moderate rain events during spring and winter seasons could release Pb, As, Cu, Zn, and Ca from agricultural areas of the watershed (0.83–12.8%; total 1545 km^2) along with SPM and SIPM into the sound. The higher concentration of Pb, As, Cu, Zn, and Ca in the spring and winter of 2018 can also be due to the less dilutionary effect in the sound waters related to moderate precipitation and a higher load of SPM and SPIM. Nevertheless, the association of HIX and NO_2^- with the spring 2018 sample scores was weak; their association could be indicative of reducing conditions as the result of the humification of terrestrial humic-like organic matter. Although there was not much difference in the amount of precipitation during summer 2018 and summer 2019, the physical separation of samples (scores) of the two summers could be due to the higher amount of river discharge including the Bonnet Carré Spillway opening during summer 2019. While comparing summer 2019 scores with the rest of the sample scores of 2018, the presence of the higher amount of protein-like component C3 and its association with DOC, FI, BIX, temperature, PO_4^{3-}, and NO_3^- suggest higher agal growth and microbial activity as the result of high nutrient input and ambient summer temperature. Besides, high algal and microbial activity can generate a high amount of fresh, biologically labile, autochthonous tryptophan-like, or protein-like DOM composition (C3) (Nguyen et al., 2005). Additionally, higher temperature along with a high amount of biological activity and higher wind action could be the reason for the increase in the concentration of CO_2 in the waters of the Western Mississippi sound during summer of 2019. Furthermore, the strong association of both NH_4^+ and Mn during summer 2019 sample scores could be either due to more reducing conditions or

the associated release of Mn from the sound bottom sediments. Similar observations about the presence of reducing conditions were also identified in adjacent coastal water bodies (Joung & Shiller, 2016; Sankar et al., 2019a). The adjacent positioning of the loadings of U, SPOM, SR, and E2:E3 for summer 2018 sample scores suggests the presence of relatively higher amount of low molecular weight organic matter in SPOM and the existence of U-DOM complex during summer 2018. Overall inclusive relationship of carbonate system parameters such as TA, DIC, and pH loadings, their PCA bearings, and their affinity with both summer 2019 and 2018 suggests their higher input into the Mississippi Sound during summer months as the dissolved load from weathering of carbonate rocks of inland Gulf Coast deposits. Additionally, Spearman's rank correlation of winter 2018 subset reaffirms the association between Cu, Ca, As, Pb, and U and SPM and SPIM, suggesting their co-transport and higher delivery during winter 2018. The inverse relationship of Mn with SPM, SPIM, SPOM, and all other elements suggests a separate source for Mn, which includes the possibility of occasional (seasonal) release from sound bottom sediments under reducing conditions. A significant positive correlation ($p < 0.05$) of SPM and SPIM suggests that a major part of SPM is inorganic in nature.

The present study used multiple variables from both inland watersheds bordering the study area as well as from the waters of the Western Mississippi Sound over the oyster bed to evaluate the factors controlling water quality. A comprehensive evaluation of seasonal change in water quality over the oyster reef in the Western Mississippi Sound indicates that the combination of local weather, hydrology, geology, land use land cover, and watershed-biogeochemical mechanisms influences its water quality. The results suggest that precipitation events affect the mobility of both dissolved and particulate constituents from different land-use and land-cover areas of the watersheds and their delivery into the Western Mississippi Sound through the river systems. Additionally, the study also indicates that water temperature and the dissemination of inland dissolved and particulate loads into the sound waters through river discharge cause changes in salinity, water chemistry, and biological activity in the waters over the oyster reef. Although present research has identified the influence of local weather and hydrology on water quality including, trace element and nutrient toxicity (concentrations above water quality criteria), DOM compositional change, and acidification over the oyster reef in the Western Mississippi sound, none of the water quality parameters (National Recommended Water Quality Criteria for Aquatic Life, EPA) seems to be extreme except for arsenic (EPA limit, 36–69 μgL^{-1}) and copper (EPA limit, 3.1–4.8 μgL^{-1}) during any of the seasons affecting higher rate of oyster mortality in the Western Mississippi Sound. This leaves us a question as to whether any instantaneous change in water quality of the Western Mississippi Sound as a result of frequent and abrupt changes in any of the above-mentioned variables causes higher oyster mortality in this region. Such recurring and instantaneous regional changes in the water quality of the Western Mississippi Sound could be caused by separate or combined effects of anthropogenic and natural causes. Some of the natural and anthropogenic events that could affect the instantaneous change in water quality of the Western Mississippi Sound could be seasonal algal blooms causing algal toxicity and associated bottom hypoxia, storms and hurricanes, the opening of Bonnet Carré Spillway, dredging activities for port operations, and dredging for the oyster fishery. The involvement of their combined or separate action could alter the water quality of the region by a rapid surge in turbidity and thus decreasing the dissolved oxygen in the waters of this region. The prevalence of prolonged higher turbidity and lower dissolved oxygen levels in the coastal waters could cause a high rate of oyster mortality (Lunt & Smee, 2014; Sarinsky et al., 2005). Bonnet Carré Spillway was opened once in spring 2018 (March 8th to 30th) and twice during spring through summer of 2019 (27th February 2019 to 11th April 2019 and 10th May 2019 to 27th July 2019). Two of our field campaigns, one during spring 2018 and another during summer 2019 coincided with Bonnet Carré Spillway openings. Unusually low salinity observed during these periods was due to the effect of Bonnet Carré Spillway freshwater discharge, which could have had an adverse effect on the health of oyster reefs. Nonetheless, we have observed a slightly higher amount of precipitation (5.69 mm) and lower discharge (206 m^3s^{-1}) during 2018 opposed to 2019 (4.91 mm and 268 m^3s^{-1}). The higher discharge could have caused dilutionary effects on the concentration of trace elements and SPM compared to the nutrients and carbonate system

parameters in the study area during 2019 compared to 2018. This could be one of the reasons why the summer 2019 dataset was distinct from the 2018 dataset. Additionally, a few samples had higher concentration of NO_3^- and NO_2^- during spring 2018 compared to the other seasons, which reaffirms the interpretation that both higher precipitation, multiple spillway openings, and less dilutionary effects during 2018 caused higher presence of nitrogen-containing compounds in the study area. With all, the present study emphasizes that instances of any such extreme events occurring in this region could adversely affect oyster health.

Conclusions and considerations

This study presents a comprehensive examination of seasonality in water quality parameters including trace elements, nutrients, DOM, coastal acidification, and SPM over the waters of the biggest deteriorating oyster reef in Western Mississippi Sound. The results demonstrated a strong seasonal change in water quality, which was found to be controlled by local weather, hydrology, watershed land use land cover, inland geology, and biological activity in the Western Mississippi Sound. It was found that the concentrations of trace elements including Pb, As, Cu, Zn, and Ca (major element) were higher along with higher amounts of terrestrial humic-like DOM compositions, SPM, and SPIM during spring and winter of 2018 suggesting SPM-trace element association and their co-transport. Contrarily, the higher amount of algal or microbially derived tryptophan-like or protein-like components along with higher amount of nutrients including PO_4^{3-}, NO_3^-, and DOC were observed over the waters of the study area during summer of 2019. Higher amount of precipitation along with dissolution and transport of fertilizers applied to agricultural areas of the inland watersheds and dissolved nutrient input from the Bonnet Carré Spillway and its subsequent delivery to the Western Mississippi Sound through river discharge caused excessive algal growth. Similarly, the higher amount of U and SPOM and low molecular weight organic compounds in the waters were identified during summer 2018. While considering seasonal variation in carbonate system parameters, TA, DIC, pH, and HCO_3^- were higher during both summer 2018 and 2019, implying the higher rate of weathering and dissolution of inland carbonate rocks of gulf coast deposits and its subsequent delivery to the sound waters. Additionally, the thermodynamic stability of $CaCO_3$ in the waters of the study area was always supersaturated (Ω_{Ca}, and $\Omega_{Ar} > 1$) and showed minimal seasonal change. Although dissolved and undissolved constituents had a conservative mixing behavior, the nutrients; trace elements including Mn and Pb; most of the carbonate system parameters including pCO_2, CO_2, pH, HCO_3^-, CO_3^{2-}, Ω_{Ca}, and Ω_{Ar}; and DOM-PARAFAC compositions C1, C2, and C3 showed no definite enrichment or depletion trend against salinity.

Although there was a seasonal change in water quality of the Western Mississippi Sound, instantaneous anthropogenic or natural events such as prolonged and occasional freshwater input from Bonnet Carré Spillway, seasonal algal blooms associated toxicity and bottom hypoxia, severe storms, dredging activities for port operations, and dredging for oyster fishery could affect the sudden change in water quality, which can be detrimental to the health of the oyster reefs. Our fieldwork during the instances of Bonnet Carré Spillway opening reinforces the idea that sudden instances of low salinity may be causing large-scale oyster mortality in the study region. For this reason, based on the present study, our recommendation is to deploy in situ water sensors to continuously monitor both seasonal and instantaneous changes in water quality to evaluate the causes of the deterioration of the oyster reefs in the Western Mississippi Sound.

Acknowledgements The authors are thankful to Rusch Ragland, Ankita Katkar, and Jannatul Ferdush of the Department of Geosciences and David Young, Logan Renz, Cary Daniel McCraine, and Jonathan Harris of Geosystems Research Institute (GRI), Mississippi State University, for their assistance with sample collection from field sites. The authors are also thankful to Dr. Rinat Gabitov of the Department of Geosciences, Mississippi State University, and Dr. Najid Hussain of the Department of Geological Sciences, University of Delaware, for their valuable help in running the CO2SYS program.

Funding This project was paid for with federal funding from the Mississippi Department of Environmental Quality and the Department of the Treasury under the Resources and Ecosystems Sustainability, Tourist Opportunities, and Revived Economies of the Gulf Coast States Act of 2012 (RESTORE Act).

Data availability All data generated or analyzed during this study are included in this published article and its

supplementary information file in the form of figures and tables. Additional information about the dataset or the dataset in a different format than what is presented in this article can be obtained from the corresponding author upon request.

Declarations

Conflict of interest The authors declare no competing interests.

Disclaimer The statements, findings, conclusions, and recommendations are those of the author(s) and do not necessarily reflect the views of the Mississippi Department of Environmental Quality or the Department of the Treasury. Any use of trade, firm, or product names is for descriptive purposes only and does not imply endorsement by the US Government.

References

Alexander, R. B., Smith, R. A., Schwarz, G. E., Boyer, E. W., Nolan, J. V., & Brakebill, J. W. (2008). Differences in phosphorus and nitrogen delivery to the Gulf of Mexico from the Misssissippi River Basin. *Environmental Science & Technology, 42*(3), 822–830.

Andrews, J. D. (1984). Epizootiology of diseases of oysters (Crassostrea virginica), and parasites of associated organisms in eastern North America. *Helgoländer Meeresuntersuchungen, 37*(1–4), 149–166. https://doi.org/10.1007/BF01989300

Andrews, J. D., & Hewatt, W. G. (1967). Oyster mortality studies in Virginia. II. The fungus disease caused by Dermocystidium marinum in oysters of Chesapeake Bay. *Chesapeake Science, 8*(1), 1–13.

Balls, P. W. (1990). Distribution and composition of suspended particulate material in the clyde estuary and associated sea lochs. *Estuarine, Coastal and Shelf Science, 30*(5), 475–487. https://doi.org/10.1016/0272-7714(90)90068-3

Beccasio, A. D. (1982). *Gulf Coast ecological inventory user's guide and information base*. Washington, DC. https://doi.org/10.2172/6750095

Beck, M. W., Brumbaugh, R. D., Airoldi, L., Carranza, A., Coen, L. D., Crawford, C., et al. (2011). Oyster reefs at risk and recommendations for conservation, restoration, and management. *BioScience, 61*(2), 107–116. https://doi.org/10.1525/bio.2011.61.2.5

Bianchi, T. S., Wysocki, L. A., Stewart, M., Filley, T. R., & McKee, B. A. (2007). Temporal variability in terrestrially-derived sources of particulate organic carbon in the lower Mississippi River and its upper tributaries. *Geochimica Et Cosmochimica Acta, 71*(18), 4425–4437. https://doi.org/10.1016/j.gca.2007.07.011

Brooks, S. J., Bolam, T., Tolhurst, L., Bassett, J., La Roche, J., Waldock, M., et al. (2007). Effects of dissolved organic carbon on the toxicity of copper to the developing embryos of the pacific oyster (Crassostrea gigas). *Environmental Toxicology and Chemistry, 26*(8), 1756–1763. https://doi.org/10.1897/06-460R1.1

Cai, W. J., Hu, X., Huang, W.-J., Murrell, M. C., Lehrter, J. C., Lohrenz, S. E., et al. (2011). Acidification of subsurface coastal waters enhanced by eutrophication. *Nature Geoscience, 4*(11), 766–770. https://doi.org/10.1038/ngeo1297

Cai, W. J., Huang, W. J., Luther, G. W., Pierrot, D., Li, M., Testa, J., et al. (2017). Redox reactions and weak buffering capacity lead to acidification in the Chesapeake Bay. *Nature Communications, 8*(1). https://doi.org/10.1038/s41467-017-00417-7

Cambazoglu, M. K., Soto, I. M., Howden, S. D., Dzwonkowski, B., Fitzpatrick, P. J., Arnone, R. A., et al. (2017). Inflow of shelf waters into the Mississippi Sound and Mobile Bay estuaries in October 2015. *Journal of Applied Remote Sensing, 11*(3), 032410. https://doi.org/10.1117/1.jrs.11.032410

Chen, R. F., & Gardner, G. B. (2004). High-resolution measurements of chromophoric dissolved organic matter in the Mississippi and Atchafalaya River plume regions. *Marine Chemistry, 89*(1–4), 103–125. https://doi.org/10.1016/j.marchem.2004.02.026

Dalrymple, R. M., Carfagno, A. K., & Sharpless, C. M. (2010). Correlations between dissolved organic matter optical properties and quantum yields of singlet oxygen and hydrogen peroxide. *Environmental Science & Technology, 44*(15), 5824–5829. https://doi.org/10.1021/Es101005u

Dash, P., Silwal, S., Ikenga, J. O., Pinckney, J. L., Arslan, Z., & Lizotte, R. E. (2015). Water quality of four major lakes in Mississippi, USA: Impacts on human and aquatic ecosystem health. *Water (Switzerland), 7*(9), 4999–5030. https://doi.org/10.3390/w7094999

Dickson, A. G. (1990). Standard potential of the reaction: AgCl(s) + 1 2H2(g) = Ag(s) + HCl(aq), and and the standard acidity constant of the ion HSO4- in synthetic sea water from 273.15 to 318.15 K. *The Journal of Chemical Thermodynamics, 22*(2), 113–127. https://doi.org/10.1016/0021-9614(90)90074-Z

Dickson, A. G., & Millero, F. J. (1987). A comparison of the equilibrium constants for the dissociation of carbonic acid in seawater media. *Deep Sea Research Part A, Oceanographic Research Papers, 34*(10), 1733–1743. https://doi.org/10.1016/0198-0149(87)90021-5

Dyer, J., & Mercer, A. (2013). Assessment of spatial rainfall variability over the lower Mississippi river alluvial valley. *Journal of Hydrometeorology, 14*(6), 1826–1843. https://doi.org/10.1175/JHM-D-12-0163.1

Faust, D. R., Kröger, R., Omer, A. R., Hogue, J., Czarnecki, J. M. P., Baker, B., et al. (2018). Nitrogen and organic carbon contents of agricultural drainage ditches of the Lower Mississippi Alluvial Valley. *Journal of Soil and Water Conservation, 73*(2), 179–188. https://doi.org/10.2489/jswc.73.2.179

Feely, R. A., Sabine, C. L., Byrne, R. H., Millero, F. J., Dickson, A. G., Wanninkhof, R., et al. (2012). Decadal changes in the aragonite and calcite saturation state of the Pacific Ocean. *Global Biogeochemical Cycles, 26*(3), 1–15. https://doi.org/10.1029/2011GB004157

García-Rico, L., Wilson-Cruz, S., Frasquillo-Félix, M. C., & Jara-Marini, M. E. (2003). Total metals in intertidal surface sediment of oyster culture areas Insonora, Mexico. *Bulletin of Environmental Contamination and Toxicology, 70*(6), 1235–1241. https://doi.org/10.1007/s00128-003-0114-1

Guy, H. P., & Norman, V. W. (1970). Field methods for measurement of fluvial sediment: U.S. Geol. Survey Techniques of Water Resources Investigations, Book 3, Chap. C2, 59 p.

Häder, D. P., Kumar, H. D., Smith, R. C., & Worrest, R. C. (2007). Effects of solar UV radiation on aquatic ecosystems and interactions with climate change. *Photochemical*

and Photobiological Sciences, 6(3), 267–285. https://doi.org/10.1039/b700020k

Hagy, J. D., Boynton, W. R., Keefe, C. W., & Wood, K. V. (2004). Hypoxia in Chesapeake Bay, 1950–2001: Long-term change in relation to nutrient loading and river flow. *Estuaries, 27*(4), 634–658. https://doi.org/10.1007/BF02907650

Hansen, A. M., Kraus, T. E. C., Pellerin, B. A., Fleck, J. A., Downing, B. D., & Bergamaschi, B. A. (2016). Optical properties of dissolved organic matter (DOM): Effects of biological and photolytic degradation. *Limnology and Oceanography, 61*(3), 1015–1032. https://doi.org/10.1002/lno.10270

Ho, P., Shim, M. J., Howden, S. D., & Shiller, A. M. (2019). Temporal and spatial distributions of nutrients and trace elements (Ba, Cs, Cr, Fe, Mn, Mo, U, V and Re) in Mississippi coastal waters: Influence of hypoxia, submarine groundwater discharge, and episodic events. *Continental Shelf Research, 175*, 53–69. https://doi.org/10.1016/j.csr.2019.01.013

Hu, X., Pollack, J. B., McCutcheon, M. R., Montagna, P. A., & Ouyang, Z. (2015). Long-term alkalinity decrease and acidification of estuaries in northwestern gulf of Mexico. *Environmental Science and Technology, 49*(6), 3401–3409. https://doi.org/10.1021/es505945p

Johannesson, K. H., Palmore, C. D., Fackrell, J., Prouty, N. G., Swarzenski, P. W., Chevis, D. A., et al. (2017). Rare earth element behavior during groundwater–seawater mixing along the Kona Coast of Hawaii. *Geochimica Et Cosmochimica Acta, 198*, 229–258. https://doi.org/10.1016/j.gca.2016.11.009

Jokinen, S. A., Jilbert, T., Tiihonen-Filppula, R., & Koho, K. (2020). Terrestrial organic matter input drives sedimentary trace metal sequestration in a human-impacted boreal estuary. *Science of the Total Environment, 717*, 137047. https://doi.org/10.1016/j.scitotenv.2020.137047

Joung, D. J., & Shiller, A. M. (2016). Temporal and spatial variations of dissolved and colloidal trace elements in Louisiana Shelf waters. *Marine Chemistry, 181*, 25–43. https://doi.org/10.1016/j.marchem.2016.03.003

Kennicutt, M. C. (2017). *Water quality of the Gulf of Mexico. Habitats and biota of the Gulf of Mexico: Before the deepwater horizon oil spill* (Vol. 1). https://doi.org/10.1007/978-1-4939-3447-8_2

Keppel, A. G., Breitburg, D. L., & Burrell, R. B. (2016). Effects of co-varying diel-cycling hypoxia and pH on growth in the juvenile eastern oyster, Crassostrea virginica. *PLoS ONE, 11*(8), 1–31. https://doi.org/10.1371/journal.pone.0161088

Koukina, S., & Lobus, N. (2018). Trace elements in suspended particulate matter and sediments of the Cai River: Nha Trang Bay estuarine system (South China Sea). *Trace Elements - Human Health and Environment*, (September). https://doi.org/10.5772/intechopen.76471

Kuwabara, J. S., Chang, C. C. Y., Cloern, J. E., Fries, T. L., Davis, J. A., & Luoma, S. N. (1989). Trace metal associations in the water column of South San Francisco Bay, California. *Estuarine, Coastal and Shelf Science, 28*(3), 307–325. https://doi.org/10.1016/0272-7714(89)90020-6

La Peyre, M., Furlong, J., Brown, L. A., Piazza, B. P., & Brown, K. (2014). Ocean & Coastal Management Oyster reef restoration in the northern Gulf of Mexico : Extent, methods and outcomes. *Ocean and Coastal Management, 89*, 20–28. https://doi.org/10.1016/j.ocecoaman.2013.12.002

La Peyre, M. K., Eberline, B. S., Soniat, T. M., & La Peyre, J. F. (2013). Differences in extreme low salinity timing and duration differentially affect eastern oyster (Crassostrea virginica) size class growth and mortality in Breton Sound, LA. *Estuarine, Coastal and Shelf Science, 135*, 146–157. https://doi.org/10.1016/j.ecss.2013.10.001

Lafabrie, C., Major, K. M., Major, C. S., & Cebrián, J. (2011). Arsenic and mercury bioaccumulation in the aquatic plant, Vallisneria neotropicalis. *Chemosphere, 82*(10), 1393–1400. https://doi.org/10.1016/j.chemosphere.2010.11.070

Lu, Y. H., Bauer, J. E., Canuel, E. A., Chambers, R. M., Yamashita, Y., Jaffé, R., & Barrett, A. (2014a). Effects of land use on sources and ages of inorganic and organic carbon in temperate headwater streams. *Biogeochemistry, 119*(1–3), 275–292. https://doi.org/10.1007/s10533-014-9965-2

Lu, Y. H., Canuel, E. A., Bauer, J. E., & Chambers, R. M. (2014b). Effects of watershed land use on sources and nutritional value of particulate organic matter in temperate headwater streams. *Aquatic Sciences, 76*(3), 419–436. https://doi.org/10.1007/s00027-014-0344-9

Lunt, J., & Smee, D. L. (2014). Turbidity influences trophic interactions in estuaries. *Limnology and Oceanography, 59*(6), 2002–2012. https://doi.org/10.4319/lo.2014.59.6.2002

McKnight, D. M., Boyer, E. W., Westerhoff, P. K., Doran, P. T., Kulbe, T., & Andersen, D. T. (2001). Spectrofluorometric characterization of dissolved organic matter for indication of precursor organic material and aromaticity. *Limnology and Oceanography, 46*(1), 38–48. https://doi.org/10.4319/lo.2001.46.1.0038

Mehrbach, C., Culberson, C. H., Hawley, J. E., & Pytkowicx, R. M. (1973). Measurement of the apparent dissociation constants of carbonic acid in seawater at atmospheric pressure. *Limnology and Oceanography, 18*(6), 897–907. https://doi.org/10.4319/lo.1973.18.6.0897

Milliman, J. D. (2001). River inputs. *Encyclopedia of Ocean Sciences*. https://doi.org/10.1006/rwos.2001.0074

Mississippi Department of Environmental Quality. (2015). *The Mississippi Gulf Coast Restoration Plan. Mississippi Department of Environmental Quality 2015 National Fish and Wildlife Foundation*.

Nguyen, M. -L., Westerhoff, P., Baker, L., Hu, Q., Esparza-Soto, M., & Sommerfeld, M. (2005). Characteristics and reactivity of algae-produced dissolved organic carbon. *Journal of Environmental Engineering, 131*(11), 1574–1582. https://doi.org/10.1061/(asce)0733-9372(2005)131:11(1574)

Ohno, T. (2002). Fluorescence inner-filtering correction for determining the humification index of dissolved organic matter. *Environmental Science and Technology, 36*(4), 742–746. https://doi.org/10.1021/es0155276

Parlanti, E., Wo, K., Geo, L., & Lamotte, M. (2000). Dissolved organic matter fuorescence spectroscopy as a tool to estimate biological activity in a coastal zone submitted to anthropogenic inputs. *Organic Geochemistry, 31*(12), 1765–1781. https://doi.org/10.1016/S0146-6380(00)00124-8

Parra, S. M., Sanial, V., Boyette, A. D., Cambazoglu, M. K., Soto, I. M., Greer, A. T., et al. (2020). Bonnet Carré Spillway freshwater transport and corresponding biochemical properties in the Mississippi Bight. *Continental Shelf Research, 199*, 104114. https://doi.org/10.1016/j.csr.2020.104114

Paul, V., Vattikuti, S., Dash, P., & Arslan, Z. (2021). Evaluating hydrogeochemical characteristics of groundwater and surface water in the Upper Pearl River Watershed, USA. *Environmental Monitoring and Assessment, 193*(5), 1–18. https://doi.org/10.1007/s10661-021-09045-7

Powell, E. N., Klinck, J. M., Hofmann, E. E., & McManus, M. A. (2003). Influence of water allocation and freshwater inflow on oyster production: A hydrodynamic-oyster population model for Galveston Bay, Texas, USA. *Environmental Management, 31*(1), 100–121. https://doi.org/10.1007/s00267-002-2695-6

Rabalais, N. N., Turner, R. E., & Wiseman, W. J. (2002). Gulf of Mexico hypoxia, a.k.a. "The dead zone." *Annual Review of Ecology and Systematics, 33*, 235–263. https://doi.org/10.1146/annurev.ecolsys.33.010802.150513

Rajagopal, S., Van Der Velde, G., Jansen, J., Van Der Gaag, M., Atsma, G., Janssen-Mommen, J. P. M., et al. (2005). Thermal tolerance of the invasive oyster Crassostrea gigas: Feasibility of heat treatment as an antifouling option. *Water Research, 39*(18), 4335–4342. https://doi.org/10.1016/j.watres.2005.08.021

Regnier, P., & Wollast, R. (1993). Distribution of trace metals in suspended matter of the Scheldt estuary. *Marine Chemistry, 43*(1–4), 3–19. https://doi.org/10.1016/0304-4203(93)90212-7

Renforth, P., & Henderson, G. (2017). Assessing ocean alkalinity for carbon sequestration. *Reviews of Geophysics, 55*(3), 636–674. https://doi.org/10.1002/2016RG000533

Runner, M. S., & Floyd, T. (2002). Water quality monitoring and Data collection in the Mississippi Sound. *53 rd Gulf and Caribbean Fisheries Institute*, 681–688.

R Core Team. (2016). R: A language and environment for statistical computing. R Foundation for Statistical Computing, Vienna, Austria.

Sankar, M. S., Dash, P., Lu, Y., Mercer, A. E., Turnage, G., Shoemaker, C. M., et al. (2020). Land use and land cover control on the spatial variation of dissolved organic matter across 41 lakes in Mississippi, USA. *Hydrobiologia, 847*, 1159–1176. https://doi.org/10.1007/s10750-019-04174-0

Sankar, M. S., Dash, P., Lu, Y. H., Paul, V., Mercer, A. E., Arslan, Z., et al. (2019a). Dissolved organic matter and trace element variability in a blackwater-fed bay following precipitation. *Estuarine, Coastal and Shelf Science, 231*, 106452. https://doi.org/10.1016/j.ecss.2019.106452

Sankar, M. S., Dash, P., Singh, S., Lu, Y. H., Mercer, A. E., & Chen, S. (2019b). Effect of photo-biodegradation and biodegradation on the biogeochemical cycling of dissolved organic matter across diverse surface water bodies. *Journal of Environmental Sciences, 77*, 130–147. https://doi.org/10.1016/j.jes.2018.06.021

Sarinsky, G., Carroll, M. A., Nduka, E., & Catapane, E. J. (2005). Growth and survival of the American oyster Crassostrea virginica in Jamaica Bay, New York. *In Vivo, 27*(1), 15–26.

Sellner, K. G., Doucette, G. J., & Kirkpatrick, G. J. (2003). Harmful algal blooms: Causes, impacts and detection. *Journal of Industrial Microbiology and Biotechnology, 30*(7), 383–406. https://doi.org/10.1007/s10295-003-0074-9

Shang, P., Lu, Y. H., Du, Y. X., Jaffé, R., Findlay, R. H., & Wynn, A. (2018). Climatic and watershed controls of dissolved organic matter variation in streams across a gradient of agricultural land use. *Science of the Total Environment, 612*, 1442–1453. https://doi.org/10.1016/j.scitotenv.2017.08.322

Singh, S., Dash, P., Sankar, M. S., Silwal, S., Lu, Y. H., Shang, P., & Moorhead, R. J. (2018). Hydrological and biogeochemical controls of seasonality in dissolved organic matter delivery to a Blackwater Estuary. *Estuaries and Coasts*. https://doi.org/10.1007/s12237-018-0473-9

Singh, S., Dash, P., Silwal, S., Feng, G., Adeli, A., & Moorhead, R. J. (2017). Influence of land use and land cover on the spatial variability of dissolved organic matter in multiple aquatic environments. *Environmental Science and Pollution Research, 24*(16), 14124–14141. https://doi.org/10.1007/s11356-017-8917-5

Singh, S., Inamdar, S., Mitchell, M., & McHale, P. (2014). Seasonal pattern of dissolved organic matter (DOM) in watershed sources: Influence of hydrologic flow paths and autumn leaf fall. *Biogeochemistry, 118*(1–3), 321–337. https://doi.org/10.1007/s10533-013-9934-1

Slowey, F. J., & Hood, D. W. (1971). Copper, manganese and zinc concentrations in Gulf of Mexico waters. *Geochimica Et Cosmochimica Acta, 35*(2), 121–138. https://doi.org/10.1016/0016-7037(71)90052-4

Soletchnik, P., Ropert, M., Mazurié, J., Gildas Fleury, P., & Le Coz, F. (2007). Relationships between oyster mortality patterns and environmental data from monitoring databases along the coasts of France. *Aquaculture, 271*(1–4), 384–400. https://doi.org/10.1016/j.aquaculture.2007.02.049

Soniat, T. M. (2014). Predicting the effects of proposed Mississippi River diversions on oyster habitat quality; Application of an oyster habitat suitability index model. *Journal of Shellfish Research, 32*(3), 629. https://doi.org/10.2983/035.032.0302

Spencer, R. G. M., Aiken, G. R., Dornblaser, M. M., Butler, K. D., Holmes, R. M., Fiske, G., et al. (2013). Chromophoric dissolved organic matter export from U.S. rivers. *Geophysical Research Letters, 40*(8), 1575–1579. https://doi.org/10.1002/grl.50357

Stedmon, C. A., & Bro, R. (2008). Characterizing dissolved organic matter fluorescence with parallel factor analysis : A tutorial. *Limnology & Oceanography: Methods, 6*(3798), 572–579. https://doi.org/10.4319/lom.2008.6.572

Stolpe, B., Guo, L., Shiller, A. M., & Hassellov, M. (2010). Size and composition of colloidal organic matter and trace elements in the Mississippi River, Pearl River and the northern Gulf of Mexico, as characterized by flow field-flow fractionation. *Marine Chemistry, 118*(3–4), 119–128. https://doi.org/10.1016/j.marchem.2009.11.007

Stumpf, R. P., Culver, M. E., Tester, P. A., Tomlinson, M., Kirkpatrick, G. J., Pederson, B. A., et al. (2003). Monitoring Karenia brevis blooms in the Gulf of Mexico using satellite ocean color imagery and other data. *Harmful Algae, 2*(2), 147–160. https://doi.org/10.1016/S1568-9883(02)00083-5

Turner, A., & Millward, G. E. (2000). Particle dynamics and trace metal reactivity in estuarine plumes. *Estuarine, Coastal and Shelf Science, 50*(6), 761–774. https://doi.org/10.1006/ecss.2000.0589

Turner, R. E. (2006). Will lowering estuarine salinity increase Gulf of Mexico oyster landings? *Estuaries and Coasts, 29*(3), 345–352. https://doi.org/10.1007/BF02784984

Turner, R. E., Rabalais, N. N., & Justic, D. (2006). Predicting summer hypoxia in the northern Gulf of Mexico: Riverine N, P, and Si loading. *Marine Pollution Bulletin, 52*(2), 139–148. https://doi.org/10.1016/j.marpolbul.2005.08.012

Uppström, L. R. (1974). The boron/chlorinity ratio of deep-sea water from the Pacific Ocean. *Deep-Sea Research and Oceanographic Abstracts, 21*(2), 161–162. https://doi.org/10.1016/0011-7471(74)90074-6

USEPA. (1999). *The ecological condition of estuaries in the Gulf of Mexico*. EPA 620-R-98- 004.

van der Sloot Hans, A., Hoede, D., Hamburg, G., Woittiez, J. R. W., & van der Weijden Cornelis, H. (1990). Trace elements in suspended matter from the anoxic hypersaline Tyro and Bannock Basins (eastern Mediterranean). *Marine Chemistry, 31*(1–3), 187–203. https://doi.org/10.1016/0304-4203(90)90038-E

Waldbusser, G. G., Gray, M. W., Hales, B., Langdon, C. J., Haley, B. A., Gimenez, I., et al. (2016). Slow shell building, a possible trait for resistance to the effects of acute ocean acidification. *Limnology and Oceanography, 61*(6), 1969–1983. https://doi.org/10.1002/lno.10348

Waldbusser, G. G., Hales, B., Langdon, C. J., Haley, B. A., Schrader, P., Brunner, E. L., et al. (2015). Ocean acidification has multiple modes of action on bivalve larvae. *PLoS ONE*. https://doi.org/10.1371/journal.pone.0128376

Wang, W. X., Meng, J., & Weng, N. (2018). Trace metals in oysters: Molecular and cellular mechanisms and ecotoxicological impacts. *Environmental Science: Processes and Impacts, 20*(6), 892–912. https://doi.org/10.1039/c8em00069g

Wanninkhof, R., Barbero, L., Byrne, R., Cai, W. -J., Huang, W. -J., Zhang, J. -Z., et al. (2015). Ocean acidification along the Gulf Coast and East Coast of the USA. *Continental Shelf Research, 98*, 1–18. https://doi.org/10.1016/j.csr.2015.02.008

Weber, C. E., & Mitchell, D. (2013). Water-quality watchdogs? –A political, environmental, and socioeconomic analysis of oyster farming in Alabama. *Agrarian Frontiers, 1*(1), 1–12.

Winstead, J., & Couch, J. (1988). Enhancement of protozoan pathogen Perkinsus marinus infections in American oysters Crassostrea virginica exposed to the chemical carcinogen n-nitrosodiethylamine (DENA). *Diseases of Aquatic Organisms, 5*, 205–213. https://doi.org/10.3354/dao005205

Yamashita, Y., Scinto, L. J., Maie, N., & Jaffe, R. (2010). Dissolved organic matter characteristics across a subtropical wetland's landscape: Application of optical properties in the assessment of environmental dynamics. *Ecosystems, 13*(7), 1006–1019. https://doi.org/10.1007/s10021-010-9370-1

Yang, B., Byrne, R. H., & Wanninkhof, R. (2015). Subannual variability of total alkalinity distributions in the northeastern Gulf of Mexico. *Journal of Geophysical Research: Oceans, 120*(5), 3805–3816. https://doi.org/10.1002/2015JC010780

Yu, H., Liang, H., Qu, F., Han, Z., Shao, S., Chang, H., & Li, G. (2015). Impact of dataset diversity on accuracy and sensitivity of parallel factor analysis model of dissolved organic matter fluorescence excitation-emission matrix. *Scientific Reports, 5*, 10207. https://doi.org/10.1038/srep10207

Zielinski, R. A., Foster, A. L., Meeker, G. P., & Brownfield, I. K. (2007). Mode of occurrence of arsenic in feed coal and its derivative fly ash, Black Warrior Basin, Alabam. *Fuel, 86*(4), 560–572. https://doi.org/10.1016/j.fuel.2006.07.033